

Manuscript Number: SG-D-16-00232

Title: Diachronous folding and cleavage in an intraplate setting (Central High Atlas, Morocco) determined through the study of remagnetizations

Article Type: Full Length Article

Keywords: Cretaceous remagnetization;
Cleavage;
Intraplate basin;
Central High Atlas;
Small circle intersection method.

Abstract: Remagnetizations are common in intraplate basins. When remagnetizations occur at an intermediate stage between different tectonic processes, they can be used for paleo-geometrical reconstructions and relative dating of different structures. This has a particular interest in geological frameworks where other geological markers are absent. In order to apply this methodology, it is necessary to calculate the regional remagnetization direction and subsequently to use this reference direction to restore the attitude of the beds at the moment of remagnetization acquisition. In this work, we use this methodology for dating a pervasive cleavage (whose time of formation is controversial) and the associated structures in the Central High Atlas. Paleomagnetic directions from 64 sites were used to calculate the regional remagnetization direction $D = 330.6^\circ$ / $I = 36.1^\circ$ that is coincident with the Albian-Cenomanian expected direction for NW Africa. This direction was used to restore the Mesozoic paleo-geometry of beds allowing us to analyse bedding orientation, cleavage and folding relationships between the present day and the Cretaceous geometry. After restoration we conclude that the development of cleavage postdates remagnetization, being in relation with Cenozoic basin inversion. However, the paleo-geometry shows incipient folds at Cretaceous times, which can be related to an intra-Mesozoic compressional event.

Novel approach for dating cleavage in inverted basins using widespread remagnetizations

Regional paleomagnetic direction of the Cretaceous remagnetization (100 Ma.)

Present-day and restored at 100 Ma. geological cross-sections

Better constraints about deformational history of the Central High Atlas basin

Cleavage in the High Atlas developed during the Cenozoic inversion

Diachronous folding and cleavage in an intraplate setting (Central High Atlas, Morocco)
determined through the study of remagnetizations

P. Calvin^{1,*}, A. M. Casas-Sainz², J. J. Villalaín¹, and B. Moussaid³

¹Laboratorio de Paleomagnetismo, Universidad de Burgos, Spain.

²Departamento de Ciencias de la Tierra, Universidad de Zaragoza, Spain

³Lab. de Bio-géo-sciences et ingénierie des matériaux, Ecole Normale Supérieure, Université Hassan II. Casablanca, Morocco.

*Corresponding author: Pablo Calvin (pcalvin@ubu.es). Dep. Física, Escuela Politécnica Superior, Río Vena, Universidad de Burgos, Av. Cantabria s/n, 09006 Burgos, Spain. ph. +34 947 258 900

Key words: Cretaceous remagnetization, cleavage, intraplate basin, Central High Atlas, small circle intersection method.

22

23 Remagnetizations are common in intraplate basins. When remagnetizations occur at an intermediate
24 stage between different tectonic processes, they can be used for paleo-geometrical reconstructions and
25 relative dating of different structures. This has a particular interest in geological frameworks where
26 other geological markers are absent. In order to apply this methodology, it is necessary to calculate the
27 regional remagnetization direction and subsequently to use this reference direction to restore the
28 attitude of the beds at the moment of remagnetization acquisition. In this work, we use this
29 methodology for dating a pervasive cleavage (whose time of formation is controversial) and the
30 associated structures in the Central High Atlas. Paleomagnetic directions from 64 sites were used to
31 calculate the regional remagnetization direction $D = 330.6^\circ / I = 36.1^\circ$ that is coincident with the Albian-
32 Cenomanian expected direction for NW Africa. This direction was used to restore the Mesozoic paleo-
33 geometry of beds allowing us to analyse bedding orientation, cleavage and folding relationships
34 between the present day and the Cretaceous geometry. After restoration we conclude that the
35 development of cleavage postdates remagnetization, being in relation with Cenozoic basin inversion.
36 However, the paleo-geometry shows incipient folds at Cretaceous times, which can be related to an
37 intra-Mesozoic compressional event.

38

39 1. Introduction

40

41 Defining the relationships between cleavage and folding is a classical [tool](#) in structural geology,
42 helping to decipher the tectonic evolution of orogenic areas (see e.g. Séguret, 1972; Mattauer, 1973;
43 Williams, 1985; Mitra and Yonkee, 1985; Ramsay and Huber, 1987; Marshak and Mitra, 1988;

44 Lüneburg and Lebit, 1998). This task requires the definition of the relative age of cleavage with respect
45 ~~to folding and their geometrical relationships in large-scale and small-scale folds.~~ Relative and absolute
46 dating of cleavage in partially inverted intracratonic basins containing rocks which underwent very low
47 to low metamorphic ~~evolution~~ is sometimes a difficult task. This is in relation with the generally weak
48 deformation ~~and~~ the lack of significant thermal events and/or the absence of syntectonic sediments
49 associated with particular tectonic phases.

50 Intracratonic Mesozoic basins of the western Tethys domain (Fig. 1; Iberian Peninsula and NW
51 Africa) show several examples of this problematic. In an overall view, these basins had a similar
52 evolution during Mesozoic-Cenozoic times. They are characterized by a first rifting phase during the
53 Early Triassic ~~followed by a post-rift phase in the Middle-Upper Triassic,~~ a second rifting phase during
54 the Jurassic or Early Cretaceous (having different timing in different basins), both followed by thermal
55 relaxation, post-rift stages. Finally a general event of inversion took place during the Cenozoic in all
56 these basins as the result of Africa, Iberia and Europe convergence (Gibbons and Moreno, 2002; Frizon
57 de Lamotte et al., 2008). Most of these basins, both in the Iberian and African plates, show a Mesozoic
58 remagnetization (e.g. Galdeano et al., 1989; Moreau et al., 1992; Juárez et al., 1998; Villalaín et al.,
59 2003; Soto et al., 2008; Torres-López et al., 2014; Moussaid et al., 2015; Calvín et al., in review) and
60 some of them developed cleavage to varying degrees. A particularly interesting stage in the evolution of
61 these basins is ~~the~~ Mesozoic compression and cleavage formation stage (as an intermediate
62 compressional stage within the overall extensional evolution), that has been clearly assessed in the
63 Cameros basin (Casas-Sainz and Gil-Imaz, 1998; García-Lasanta et al., 2014), and proposed in the
64 High Atlas (Laville, 1985; Laville and Piqué, 1992), having important implications in plate kinematics.
65 This Mesozoic compression event, but without cleavage development, also was recognized by Soto et
66 al. (2011) in the Basque-Cantabrian basin (N Spain).

67 Cleavage in the Cameros basin (westernmost sector of Iberian Range, N Spain) has a

68 widespread development and is related (both in time and in space) to a metamorphic event (Gil-Imaz
69 and Pocoví-Juan, 1994; Casas-Sainz and Gil-Imaz, 1998; Mata et al., 2001) as assessed from the
70 presence and relationships between pre-, syn-, and post-cleavage metamorphic minerals. The thermal
71 metamorphic peak has been dated at 99.5 ± 2.2 M.a. by Ar-Ar isotope analyses in authigenic phengite
72 (Golberg et al., 1988). However, cleavage in the Basque-Cantabrian basin seems to be associated with
73 ~~Cenozoic inversion~~ (Álvaro, 1976; Cámara, 1977; Gómez et al. 2002); for example, Oliva-Urcía et al.
74 (2013) reported a vertical cleavage in this area related to buttressing processes against an extensional
75 fault, during the Cenozoic inversion, although in this case deformation was attributed to this stage
76 based only upon geometrical criteria. A similar origin was proposed for cleavage appearing in the
77 Galve basin (central Iberian range, NE Spain), also related to buttressing against steeply-dipping
78 normal faults (Liesa et al., 2004). ~~Finally~~, other examples of cleavage-related folds were reported in the
79 western Iberian range (Gutiérrez-Elorza and Pedraza-Gilsanz, 1974; Gual-Pérez et al., 2012; García-
80 Lasanta et al., 2015) where they appear to be related to Cenozoic basin inversion.

81 Controversy about timing of cleavage formation in relation to other structures is a long-term
82 issue in the geological literature about the Central High Atlas (CHA; NW Morocco), which constitutes
83 the target of this work. A sinistral transpression phase during Late Jurassic times, coeval with intrusion
84 of magmatic bodies and an associated hydrothermal metamorphic event, has been invoked to explain
85 anomalous thermal gradients favoring cleavage development (Laville and Piqué, 1992; Laville et al.,
86 1994). Strong uplift of the Mesozoic basin associated with Jurassic compression proposed by these
87 authors was contradicted by Charrière et al. (2009), ~~dating~~ as Paleocene the supposed Callovian-Lower
88 Cretaceous sediments that lie unconformably on the igneous intrusions and host rocks. ~~Furthermore~~,
89 Barbero et al. (2007) by means of fission tracks indicated that the main uplift of these igneous rocks
90 occurred during Cenozoic times. However, although these ~~arguments~~ are in support of the absence of
91 total basin inversion during Mesozoic times, cleavage-related folding could have been generated during

92 the Mesozoic, as it occurs in the Cameros basin, without an important uplift of the basin.

93 In this paper we propose a methodological approach using paleomagnetism and the analysis of
94 remagnetization directions to the relative dating of folds and cleavage and, consequently,
95 compressional phases occurring during the evolution of inverted extensional basins. A pervasive
96 widespread remagnetization, dated around 100 M.a., has been observed in the CHA (Torres-López et
97 al., 2014; Moussaid et al., 2015). From the application of the above-mentioned method to this
98 remagnetization, we demonstrate that cleavage in the CHA was generated during the Cenozoic
99 compression, after the remagnetization stage, although some Mesozoic compressional folds formed in
100 the area before remagnetization times. Moreover, since remagnetizations are common in intraplate
101 extensional basins where a minimum thickness of sediments was accumulated (e.g. Villalaín et al.,
102 2003, Moreau et al., 2005; Elmore et al., 2012; Van der Voo and Torsvik, 2012; Torres-López et al.,
103 2014 and references therein), it can be used for resolving tectonic and structural problems related to the
104 evolution of sedimentary basins as proposed here.

105

106 **2. Regional geological background**

107

108 The Atlas system is an intracontinental chain located in the foreland of the southernmost sector
109 of the Mediterranean Alpine System, formed as the result of the inversion of extensional Mesozoic
110 basins during the Cenozoic convergence between African and European plates (Mattaueer et al., 1977;
111 Gomez et al., 2000). The Mesozoic sedimentation in the CHA began with Triassic continental clastic
112 sediments and evaporites during the first stage of rifting, which are intercalated by Triassic-Jurassic
113 basalts. During the Early-Middle Jurassic, normal faults were reactivated in a second stage of rifting
114 and more than 5000 m of marine carbonates and fluvial red beds were accumulated (Frizon de Lamotte

115 et al., 2008). During this stage, NE-SW normal faults were generated in addition to ENE-WSW faults
116 related to the NW-SE extension, and an important diapiric activity began, forming salt-walls limiting
117 sub-basins (Saura et al., 2014). During the Late Jurassic-Early Cretaceous, the axial zone of the CHA
118 emerged, and rocks related to the basinal stage younger than the Upper Jurassic are not preserved in
119 this area.

120 The extensional stage ended with an alkaline to transitional magmatic event, characterized by
121 mafic intrusive rocks dated with K-Ar in biotite at 160 ± 3 M.a. to 152 ± 3 M.a. (Hailwood and
122 Mitchell, 1971) and with Ar-Ar in biotite at 151.3 ± 0.5 M.a. to 146 ± 0.5 M.a. (Armando, 1999).

123 The alpine compression imprinted relatively weak deformation in the CHA, with values of
124 shortening ranging between 15% and 24% (Teixell et al., 2003) in a NW-SE direction (without
125 considering internal deformation associated with cleavage). The structure of the CHA is characterized
126 by tight anticlines with steeply-dipping limbs parallel to the ENE-WSW general trend of the chain,
127 cored by Triassic shales and basalts and Jurassic gabbros, which limit wide, gentle synclines. These
128 anticlines were partially developed during the Mesozoic (Torres-López et al., 2016) primarily because
129 of diapiric processes (Bouchouata et al., 1995; Ettaki et al., 2007; Michard et al., 2011; Saura et al.,
130 2014) and also enhanced by Jurassic igneous intrusions (Calvín et al., in review). In the central sector
131 of the CHA, a pervasive foliation appears (Fig. 4) showing varying attitudes along and across the main
132 structural trends (Laville and Piqué, 1992).

133 Torres-López et al., (2014) described the presence in the CHA of an Albian-Cenomanian (≈ 100
134 M.a.) widespread remagnetization affecting the Jurassic carbonate rocks and red beds of the central part
135 of the chain. This event is responsible for the particular magnetic behavior of rocks both in the
136 demagnetization processes and in rock magnetic experiments. Because remagnetization in carbonate
137 rocks can be linked both to burial depth and regional thermal anomalies, it is restricted to the central
138 part of the High Atlas, along the basin depocenter(s) and cannot be recognized in marginal areas

139 (northern and southern margins of the CHA) of the Atlasic basin (Torres-López et al., 2014). Torres-
140 López et al. (2016) used this remagnetization to restore the attitude of the beds at the moment of its
141 acquisition.



143 3. **Geometry of cleavage and folding**

144
145 The study area covers a large part of the CHA characterized by (i) tabular areas without
146 significant structures and (ii) trains of plurikilometric folds with a constant NE-SW trend (Fig. 2). The
147 central sector of the study area is characterized by folds that can be followed along trend up to 100 km,
148 although most of them show lengths between 20 and 50 km. Many of the anticlines are cut by
149 extensional faults inherited from the rift stage and show large amounts of gabbros in their cores. These
150 faults are linked in many cases to complications of the structure and are the main responsible for the
151 interruptions of fold axes along trend. Cleavage shows an uneven distribution throughout the study area
152 (Laville and Piqué, 1992; Laville et al., 2004), probably conditioned by the sedimentary load, since it is
153 more pervasive approaching the sectors with thicker syn-rift Jurassic series. This area coincides with
154 the Mesozoic basin center, as stated from illite crystallinity studies (Schaer and Persoz, 1976; Schaer,
155 1987). Although having many complications in detail, as will be described below (see also Laville and
156 Piqué, 1992; Schaer, 1987), cleavage shows in general steep dips and runs parallel to the structures.
157 The study area can be divided into two structural domains: a central domain (Ikkou-Amouguer sector),
158 where tight anticlines are the dominant structures, and a SW domain (Timarirhine sector), a tabular
159 region without significant structures and axial-plane cleavage associated with moderately-dipping beds
160 and doubly-vergent box folds (Figs. 3 and 4).

161
162 The present-day geometry of the Timarirhine sector is characterized by a tabular, subhorizontal

163 disposition interrupted by (i) large-scale folds with gentle limb dips, showing amplitudes of hundreds
164 of meters and wavelengths of a few kilometers (e.g. Timarirhine anticline) and (ii) deca- to hectometric
165 structures, mainly folds and thrusts. These include doubly-vergent box anticlines having angular hinges
166 (Fig. 3a) and limbs dipping about 50°. Amplitude of these anticlines rarely exceeds 100 m. Some
167 thrusts appear in the area, either in relation with the cores of the folds or involving individual beds or
168 groups of beds with subhorizontal attitude (Fig. 3b), favored by the existence of many incompetent
169 levels within the Jurassic series. A pervasive cleavage can be recognized in soft and hard lithologies,
170 showing pressure-solution features in calcareous rocks (Fig. 4a, b and Fig. 5) whereas slaty cleavage
171 dominates in marls and shales (Fig. 4c, d). Cleavage shows in general steep dips, and high or low
172 angles to bedding, depending on the dip of beds (Fig. 5). Cleavage refraction is common at the
173 transition between marly and calcareous units (Fig. 4e). Folds do not show a dominant vergence,
174 although a prevalent southward dip of cleavage can be interpreted from the complete dataset (Fig. 6).

175 The Tissila-Amouguez sector is characterized by tight, kilometer-scale anticlines (Fig. 3c)
176 separated by wider synclines (Fig. 3d), sometimes with angular hinges (Fig. 3e), in whose cores Middle
177 Jurassic red beds crop out. Although fold trend orientation is relatively constant, numerous changes of
178 strike of beds, linked to re-activation of extensional normal faults, periclinal axes and relays between fold
179 axes can be observed in the geological map (Fig. 2). Some of these changes, especially those regarding
180 E-W striking beds have been classically attributed to interference between NE-SW and E-W folding
181 stages (De Sitter, 1976). In some of the synclines, a kink-fold geometry, with straight limbs having
182 homogenous dips, and angular hinges, can be observed (Fig. 3e). Rounded hinges are more common
183 near the periclinal termination of folds. In general, a combination of both kink and flexural geometries
184 can be inferred from fold reconstruction. Cleavage appears discontinuously, more pervasive when
185 approaching the core of anticlines and seldom in the Bathonian-Callovian red beds cropping out at the
186 cores of the synclines. The Ikkou syncline is a remarkable exception to this rule, since pervasive

187 subvertical cleavage (Fig. 4c) can be observed along the red beds at its core (mainly in its Southern
188 limb). Cleavage and bedding show in general similar strikes, almost parallel when dips of beds are
189 steeper than 60°, ~~and can also strike perpendicular~~ to each other in some particular places near the fold
190 periclines (Fig. 6).

191 Bedding-cleavage relationships indicate both layer-parallel shortening (cleavage perpendicular
192 to bedding in shallow-dipping layers) and flattening combined with flexural-flow processes (cleavage
193 defining reverse fans at the limbs of folds, independently of refraction geometries) as the main
194 mechanisms of cleavage formation (Fig. 4). Their relative contribution depends on the mechanical
195 stratigraphy and the dip of the sedimentary sequence. Cleavage associated with flexural-flow is
196 dominant at fold limbs and thick, incompetent beds, delineating the axial planes of folds at the acute
197 bisector between cleavage attitude at both limbs. Vertical cleavage appears in sub-horizontal beds as
198 result of layer-parallel shortening. Hectometer-scale, secondary anticlines located at the limbs of the
199 main folds allowed us to determine genetic relationships between cleavage and folding more accurately
200 than when dealing with kilometer-scale folds. Locally, and especially in thick shaly units, cleavage can
201 be affected by kink-bands generally indicating late, normal shear movements.

202 Because of their especial relevance in relation to remagnetization, we have focused in the study
203 of cleavage origin in limestones occurring along the sedimentary sequence. Cleavage ~~geometry~~ in thin-
204 sections in limestones shows a pressure-solution behavior (Fig. 5), with different degrees of
205 development from short, discontinuous planes characterized by the accumulation of iron oxides in
206 rocks without evidences of macroscopic cleavage at the outcrop scale (Fig. 5a, b and c) to an almost
207 continuous cleavage and extremely thin microlithons (Fig. 5d, e and f). Some samples show an “en
208 echelon” disposition of the cleavage planes (Fig. 5b, d) indicating simple-shear processes related to
209 flexural-flow. It is remarkable the absence of phyllosilicates related with the cleavage, being
210 carbonates, quartz, iron oxides, iron sulphides and organic matter the only components of the

211 limestones. Pyrites are not related to cleavage and probably they were formed during the early
212 diagenetic stages.

213

214 **4. Methodology of paleomagnetic analysis**

215

216 **4.1. Sampling and paleomagnetic measurements**

217

218 Forty-three new sites were sampled (Fig. 2 and supplementary data; 44 sites in Jurassic
219 carbonate rocks, namely marls and limestones, and two in red beds), taking at least eight cores per site
220 with a gasoline-powered machine. In addition to the paleomagnetic sites, bedding and cleavage were
221 also measured in 26 additional structural sites. Paleomagnetic analyses were conducted on 360 samples
222 using a 2G cryogenic magnetometer at the Paleomagnetic Laboratory of the University of Burgos
223 (Spain), which integrates Alternating Field (AF) coils. Stepwise thermal (Th) demagnetization was
224 conducted with a TD48-DC thermal demagnetizer. 6 to 16 steps were taken from room temperature up
225 to 450-500 °C for limestones and to 670 °C in red beds.

226 Paleomagnetic directional components were calculated by principal component analysis
227 (orientation and maximum angular deviation error –MAD- of the component; Kirschvink, 1980) on
228 orthogonal demagnetization diagrams using Remasoft software (Chadima and Hroda, 2006). Then, the
229 mean site directions and related statistical parameters were calculated (Fisher, 1953).

230

231 **4.2. Small Circle Intersection (SCI) method and bedding restoration**

232

233 According to Torres-Lopez et al. (2014) and Moussaid et al. (2015), carbonate rocks and red
234 beds from the CHA carry a synfolding remagnetization dated around 100 M.a.. Since the

235 remagnetization was acquired at the same moment (at geological scale) in all sites, it is possible to
236 calculate a local paleomagnetic direction for the study area using the SCI method, which is the
237 expected direction for that time (Shipunov, 1997; Henry et al., 2004; Waldhör and Appel, 2006).

238 Once the expected direction is obtained, and assuming the absence of complex rotations (e.g.
239 vertical axis rotation or two different axes of horizontal rotation, among others) after the acquisition of
240 the remagnetization, it is possible to restore the attitude of beds at the moment of the remagnetization
241 event, following the methodology explained in Villalaín et al. (2015). The optimal paleomagnetic
242 direction for each site is calculated considering the paleomagnetic direction that best approaches the
243 reference, and is assumed to be located within a small circle that links the paleomagnetic directions in
244 GEO and TILT coordinates (whose axis is the strike of bedding). Subsequently, the angle between the
245 *in situ* and the optimal paleomagnetic directions (along the small circle) can be calculated. Applying the
246 same rotation to beds, we obtain their paleodip at the moment of remagnetization (Villalaín et al., 2003;
247 Soto et al, 2008; Torres-López et al., 2016).


248 Therefore, it is possible to analyze the relationship between bedding and cleavage *in situ* and
249 after restoration at 100 M.a.. The comparison between them, together with the geometrical
250 relationships between cleavage and folds can be used to determine whether the cleavage predates or
251 postdates the remagnetization, and, therefore, whether it is related or not to pre-Cenozoic folding in the
252 CHA, the target of this work.

253 With this purpose, two detailed cross-sections were made along two key profiles (Fig 2) both
254 before and after the restoration at 100 M.a.. Furthermore, isolated keys outcrops with pre and post-
255 remagnetization folds were analyzed.

256

257 **5. Paleomagnetic directions**

258

Standard paleomagnetic analysis allowed us to calculate in each site statistically well-defined paleomagnetic directions with systematic normal polarity (Table 1) and typical unblocking temperatures between 300 °C to 450 °C in carbonates and 400/500 °C to 600/660 °C in red beds, after removal of viscous overprint and thermal alteration (Fig. 7). Both in limestones and in red beds, most samples show intensities of natural remanent magnetization (NRM) around $1-10 \times 10^{-3}$ A/m and the characteristic remanence (ChRM) represents about 30-50 % of the total NRM. In most of the limestones the ChRM goes to the origin. However, in red beds the ChRM does not pass through the origin, but it is not possible to isolate the high-temperature component because spurious components induced during heating mask the highest temperature components. Detailed magnetic properties of these rocks can be found in Torres-López et al. (2014) and Moussaid et al. (2015). 

Applying the Small Circle Intersection (SCI) method (Waldhör and Appel, 2006) to a total of 65 paleomagnetic site mean directions (44 paleomagnetic directions from this work, 9 from Torres-Lopez et al., 2014, and 12 from Calvin et al., in prep., Table 1) the direction of the remagnetization was calculated obtaining a value of $D= 330.6^\circ$ / $I= 36.1^\circ$. This direction is coincident with that obtained in two sites having horizontal bedding and also agrees with the 100 M.a. expected direction determined from the Global Apparent Polar Wander Path (GAPWP) in NW Africa coordinates (Fig. 8, Torsvik et al., 2012). The good clustering of the best fit direction (BFD) for most sites (Fig. 8c) indicates the absence of complex rotations that could preclude the application of this method. However, some sites show angles between the BFD and the expected direction larger than 10° (Table 1), mainly sites of the Outerbat-Amougou sector. These sites should be analyzed carefully.

279

280 **6. Restoration of the structure at 100 M.a. and relation with cleavage**

281

Two detailed cross-sections were restored using paleomagnetic data (Table 1) to their 100 M.a.

283 geometry (Fig. 9). Both cross-sections, having a length of 5 and 15 km respectively, have been drawn
284 considering foliation and its geometrical relationships with bedding in two representative areas of the
285 studied structures: the tabular geometry of the Timarirhine sector, showing folds with kink geometry
286 and the Ikkou syncline, in whose core the Middle Jurassic red beds crop out. Furthermore, a detailed
287 map of the Outerbat sector, where 3D geometrical relationships between bedding and cleavage are
288 spectacularly depicted, were also analyzed.

289

290 The cross-section in the Timarirhine sector (Fig. 9a) shows a flat geometry with a South-
291 dipping envelope and box-fold anticlines. Cleavage shows both northwards and southwards dips and
292 appears both in the flat areas and at the limbs of the anticlines. Cleavage is particularly pervasive at
293 both walls of high-angle reverse faults located at the middle of the cross-section. The 100 M.a.
294 geometry (Fig. 9a) obtained from the restoration of paleomagnetic vectors shows incipiently developed
295 folds with the same disposition as the current folds but with shallower dips at their limbs. The overall
296 southwards tilting of the northern part of the section ~~was horizontal at this time~~. Interestingly,
297 deformation associated with the reverse fault is absent in the palinspastic section (Figs 9a and 10a). If
298 cleavage is restored according to its present-day angular relationship with bedding, no changes occur in
299 sub-horizontal beds, but changes are significant at the limbs of folds (sites AG01, SK06 and SK05),
300 where cleavage becomes strongly oblique to their axial planes, acquiring inconsistent orientations, in
301 the restored cross-section. Differences between cleavage attitude between sites SK08 and SK09 in the
302 restored cross-section are also remarkable (Figs. 9a, 10a). This, in addition to the presence of post-
303 remagnetization folds (Fig. 10a, b) in the sector (see location in Fig. 2) showing axial plane cleavage,
304 agrees with a post-remagnetization development of the foliation.

305

306 The Tissila cross-section (Fig. 9b) depicts a wide syncline (Ikkou syncline) with a thick series

307 of Lower-Middle Jurassic in its core, limited to the north by an inverted normal fault associated with
308 diapiric activity during the extensional stage, and to the south by the asymmetric Tissila anticline (see
309 also López-Torres et al., 2016). The Ikkou syncline could be related with a buttressing process because
310 of the difficulty to fold a thick sedimentary series and the steep dips of faults at basin borders. Fault
311 inversion of the northern basin margin was also precluded by the steep dip of the normal fault at this
312 margin, and the fault would act as a buttress. Across the syncline a sub-vertical cleavage (more
313 developed in its S limb) with constant dip appears, independently of the dip of beds and slightly
314 oblique to the average axial plane of the fold. After restoration of bedding and cleavage (following the
315 same criteria applied in the Agoudal cross-section) at 100 M.a., hinge migration from South to North
316 between the Cretaceous and the Cenozoic can be inferred and cleavage shows a steep dip towards the
317 North, but more parallel to bedding. Moreover, cleavage developed around the Tissila anticline is
318 consistent with an attitude of axial-plane cleavage for the fold in its present-day stage, rather than with
319 bed attitude at 100 M.a.

320

321 The Outerbat sector (Fig. 11) is particularly interesting because bedding/cleavage relationships
322 can be analyzed in plan-view within a relatively small area. The structural map of this area shows the
323 changing attitude of cleavage and bedding, with cross-cutting relationships at the limbs of the NE-SW
324 trending fold, consistent with the axial plane but cutting perpendicular to beds at the hinge zone where
325 beds have a NW-SE strike. However, there are also dykes of Late Jurassic-Early Cretaceous age
326 (Hailwood and Mitchell, 1971) cutting across the structure and they are not folded with the beds (Fig.
327 11) indicating that the fold predates the emplacement of the dykes. As it occurs with the geometries
328 depicted in cross-sections, the 100 M.a. geometry is at an intermediate point between horizontal beds
329 and completely developed folds, thus indicating that folds were partially formed before the
330 remagnetization stage, and that its present-day geometry completely developed after flattening and

axial-plane cleavage formation, as suggested by the changes in orientation of cleavage planes that underwent subsequent folding in some parts of the structure.

Furthermore, additional information is given by a fold of the westernmost sector. Most of the deformation of this fold predates the acquisition of the remagnetization (Fig. 10c) but the cleavage was again developed after the main folding according to bedding-cleavage relationship.

7. Discussion

7.1. Remagnetization-cleavage chronological relationship

Results indicate that the restitution of the geometry at the moment of the remagnetization is a useful tool to relatively date tectonic processes in the absence of other markers. The use of this methodology in this work clearly indicates that the development of the cleavage is related with folding and it post-dates the remagnetization, solving the old discussion regarding the age of this cleavage (with the proposed hypothesis of Upper Jurassic or Cenozoic cleavage). However, since cleavage and chemical remagnetizations can be triggered for common external processes (as a regional temperature increase) or the cleavage development can generate regional remagnetization events itself, further discussion about cleavage-remagnetization relationship is necessary.

Both organic matter maturation (Brothers et al., 1996) and smectite-illite transformations (Katz et al., 2000) can generate authigenic magnetite with minimum formation temperatures around 90°C, similar in both processes (Pevear, 1999). Orogenic fluids can be the responsible for the formation of new magnetite grains (Elmore et al., 2012). On the other hand, Oliva-Urcia et al. (2008) propose a mechanism of remagnetization as result of mechanical reorientation of the magnetic grains during

355 cleavage development. Izquierdo-Llavall et al. (2013) found links between reflectance of the vitrinite,
356 illite cristallinity and cleavage, all of them in relation with the critical temperature of 140 °C for
357 cleavage development in the Pyrenees fold-and-thrust belt. In this way, and taking into account that
358 remagnetization in the High Atlas is syn-folding, we could be led to interpret remagnetization and the
359 cleavage development as co-genetic in the frame of a main tectonic phase. However, the particularly
360 fortunate conditions of the High Atlas provide two arguments that allow us to discard the link between
361 these two events. On one side, the remagnetization is recognized more widely than the cleavage both in
362 its areal extent as in its representation along the sedimentary series, what indicates that the
363 remagnetization is less restrictive ~~in~~ regard to p-T and deformation conditions (supposing that they
364 were genetically related). On the other side, the chronological relationship between remagnetization
365 and cleavage, when they can be clearly obtained from the bedding/cleavage geometrical relationships,
366 systematically show that cleavage postdates the remagnetization. If they were contemporaneous, we
367 should see that cleavage both pre and postdates the remagnetization, or else that the remagnetization
368 always postdates cleavage as it occurs in the Cameros basin (Villalaín et al., 2003; García-Lasanta et
369 al., in prep.) (since the remagnetization will be less restrictive and therefore the acquisition should ~~to~~
370 finish after cleavage development). Hence, the remagnetization can be clearly bracketed in Cretaceous
371 times, whereas cleavage development happened in the Cenozoic, related with folding during the main
372 inversion of the CHA. Therefore, we can conclude that remagnetization and cleavage are two clearly
373 different, unrelated processes, separated in time.

374 Another important question regarding this issue is the absence of phyllosilicates in some of the
375 cleaved limestones which are remagnetized. This point seems to indicate there is no relation between
376 remagnetization and illitization processes, being more important the presence of organic matter and
377 iron oxides (pyrite) in the process of the remagnetization. This also explains the absence of a
378 remagnetization related with the cleavage development since the latter is a pressure-solution cleavage

379 without important recrystallization processes involved.

380

381 7.2. Interpretation of paleomagnetic data after development of cleavage folds

382

383 Another question arising in paleomagnetic analysis in regions undergoing deformation and
384 cleavage development is the possible deformation of paleomagnetic vectors (Kingfield et al., 1983;
385 Cogné and Perroud, 1985; Hirt et al., 1986; Borradaile, 1997; Oliva-Urcía et al., 2009). In the CHA,
386 cleavage post-dates remagnetization and therefore a caveat about possible deformation of the magnetic
387 remanence can be considered. This possible deformation of the paleomagnetic vector depends of
388 different factors: (i) the intensity of the deformation of the rock, (ii) the angle between the flattening
389 direction and the paleomagnetic vectors (according to geometric relationship proposed by Ramsay and
390 Huber (1987) the deformation of remanence would be lower than the confidence angle, becoming
391 bigger for intermediate angles) and (iii) the morphology of the ferromagnetic minerals which carried
392 the magnetization (SD magnetite in this case), being anisotropic grains more likely to be rotated than
393 isomorphic grains.

394 In spite of the angle between flattening direction (according to cleavage geometry) is different
395 in different places (Fig. 9) and the variability of samples (regarding the degree of deformation), from
396 the studied samples there does not exist difference regarding paleomagnetic direction in cleaved or
397 non-cleaved rocks. One possibility is that ferromagnetic minerals within microlithons in pressure-
398 solution or slaty cleavage have not been involved in deformation. Other possibility is that the magnetic
399 grains are close to the multiaxial morphology. For the last, a more detailed study analyzing the
400 ferromagnetic fabric and the morphology of the magnetite grains in the sense of Jackson and Swanson-
401 Hysell (2012) could shed light in the future in this subject. However a magnetic behavior of the grains
402 as uniaxial no guarantee a uniaxial (anisotropic) behavior in a mechanic point of view since small

403 shape anisotropy (c/a axis relationship around 1.1) of the SD magnetite grains gives to the grains an
404 uniaxial magnetic behavior (Winklhofer et al., 1997).

405

406 **6. Conclusions**

407

408 Remagnetization in the study area shows systematically normal polarity, it has been dated as in
409 previous studies as Albian-Cenomanian (100 M.a.) and it shows a syn-folding behavior.

410 The presence of remagnetizations in intraplate basins can allow restoring the geometry of them
411 at the moment of the acquisition of the remagnetization; this methodology can help to resolve some
412 geological process. In this work some key cross-sections of the Central High Atlas are compared in the
413 present-day and the restored (at 100 Ma.) geometry in order of relatively dating the tectonic cleavage
414 (pre- or post-remagnetization) present in the area.

415 Cleavage-bedding geometrical relationships at present and at the 100 M.a. restored cross-
416 sections show that the development of cleavage clearly postdates the remagnetization acquisition.
417 Besides, geometrical relationships indicate that folding and cleavage development are genetically
418 related and there are not evidences of late folding of the cleavage. These facts support the absence of a
419 general cleavage development in the CHA before the Albian-Cenomanian and it is associated with the
420 Cenozoic basin inversion and folding. Local cleavage associated with Late Jurassic intrusions and
421 contact metamorphism (Schaer and Persoz, 1976; Laville and Piqué, 1992; Laville et al., 1994) is
422 restricted to the surroundings of the igneous bodies.

423 - Structural analyses of folds and cleavage have allowed observing different cleavage development
424 mechanism; The Timarirhine sector is a tabular area without extensional faults, and sub-horizontal
425 disposition only interrupted by box-folds (Fig. 11). Here, axial-plane cleavage can be interpreted as
426 generated both by flattening associated with flexural-flow mechanisms and layer-parallel

shortening. In this case, the geometrical relationships along the Timarirhine cross-section (and folds close to it) clearly indicate a post-remagnetization development of cleavage, related to the Cenozoic inversion of the CHA.

- A completely different scenario is the central part of the studied area, where inherited extensional faults control the subsequent compressional structure. Cleavage is sub-vertical and cleavage trajectories trend parallel to faults (as in Tissila and Outerbat sector), indicative of buttressing processes probably during the Cenozoic inversion, although this tentative chronology is not conclusive.

It is noteworthy the presence of evidences of proto-box folds in the Timarirhine area and small folds in the westernmost sector developed before the acquisition of the remagnetization. These structures cannot be related to diapiric or extensional processes in the sense of Saura et al. (2014) or to gabbroic intrusion (Calvín et al., in review) as the ones characterized by Torres-López et al. (2016). Some of which can also be observed in the cross-sections (Figs. 9b and 12) associated with basement normal faults. Precisely, the absence of deformations linked to halokinetic or igneous processes in the studied area can be the key that allows us to observe shallow pre-remagnetization dips, and this particular geometry can help to understand the whole evolution of the CHA. Theoretical, these structures could be related to transpressional processes according to Laville and Piqué (1992). However, these results have to be taken carefully because the shallow dip of beds at the flanks of the structures is close to the uncertainties of the restoration method.

Finally, the paleo-geometrical reconstruction developed from restoration of a syn-tectonic remagnetization has been demonstrated as a powerful methodology to analyze cleavage and folding history.

451 **Acknowledgments**

452

453 This study was financed by the research project CGL2012-38481 of the MINECO (Spanish Ministry of
454 Economy and Competitiveness) with also FEDER founding (European Union). Pablo Calvín also
455 acknowledges the MINECO for the F.P.I. research grant BES-2013-062988.

456

457 **References**

458 Alvaro, M., 1976. Nota sobre la presencia de dos esquistosidades en el Cretácico inferior de Bilbao
459 (Cordillera Vasco-Cantábrica). Boletín Geológico y Min. 87, 453 – 455.

460 Armando, G., 1999. Intracontinental alkaline magmatism: Geology, Petrography, Mineralogy and
461 Geochemistry of the Jebel Hayim Massif (Central High Atlas-Morocco).

462 Barbero, L., Teixell, A., Arbolea, M.-L., Río, P. Del, Reiners, P.W., Bougadir, B., 2007. Jurassic-to-
463 present thermal history of the central High Atlas (Morocco) assessed by low-temperature
464 thermochronology. Terra Nov. 19, 58 – 64. doi:10.1111/j.1365-3121.2006.00715.x

465 Borradaile, G.J., 1997. Deformation and paleomagnetism. Surv. Geophys. 18, 405 – 436.
466 doi:10.1023/A:1006555906559

467 Bouchouata, A., Canérot, J., Souhel, A., Gharib, A., 1995. Stratigraphie séquentielle et évolution
468 géodynamique du Jurassique de la région Talmest-Tazoult (Haut Atlas central, Maroc). Comptes
469 Rendus de L' Academie Des Sci. Paris 320, 749 – 756.

470 Brothers, L.A., Engel, M.H., Elmore, R.D., 1996. The late diagenetic conversion of pyrite to magnetite
471 by organically complexed ferric iron. Chem. Geol. 130, 1 – 14. doi:10.1016/0009-2541(96)00007-

472 1

- 473 Cámara, P., 1997. The Basque-Cantabrian basin's Mesozoic tectono-sedimentary evolution. Mémoires
474 la Société géologique Fr. 167 – 176.
- 475 Casas-Sainz, A.M., Gil-Imaz, A., 1998. Extensional subsidence, contractional folding and thrust
476 inversion of the eastern Cameros basin, northern Spain. Geol. Rundschau 86, 802 – 818.
477 doi:10.1007/s005310050178
- 478 Chadima, M., Hrouda, F., 2006. Remasoft 3.0 a user-friendly paleomagnetic data browser and analyzer.
479 Trav. Géophysiques 27, 20 – 21.
- 480 Charrière, A., Haddoumi, H., Mojon, P.-O., Ferrière, J., Cuche, D., Zili, L., 2009. Mise en évidence par
481 charophytes et ostracodes de l' âge Paléocène des dépôts discordants sur les rides anticlinales de
482 la région d' Imilchil (Haut Atlas, Maroc) : conséquences paléogéographiques et structurales.
483 Comptes Rendus Palevol 8, 9 – 19. doi:10.1016/j.crpv.2008.11.006
- 484 Cogné, J.-P., Perroud, H., 1985. Strain removal applied to paleomagnetic directions in an orogenic belt:
485 the Permian red slates of the Alpes Maritimes, France. Earth Planet. Sci. Lett. 72, 125 – 140.
486 doi:10.1016/0012-821X(85)90122-0
- 487 de Sitter, L.U., 1976. Structural Geology, 3rd edition. McGraw-Hill, New York.
- 488 Elmore, R.D., Muxworthy, a. R., Aldana, M., 2012. Remagnetization and Chemical Alteration of
489 Sedimentary Rocks, Geological Society, London, Special Publications. Geologic Society Special
490 Publication 371, london. doi:10.1144/SP371.15
- 491 Ettaki, M., Ibouh, H., Chellaï, E.H., Milhi, 2007. Les structures “diapiriques” liasiques du Haut-
492 Atlas central, Maroc: exemple de la ride d'Ikerzi. Africa Geosci. Rev. 14, 79 – 93.
- 493 Fisher, R.A., 1953. Dispersion on a sphere. Proc. R. Soc. London 217A, 295 – 305.

494 Frizon de Lamotte, D., Zizi, M., Missenard, Y., Hadif, M., El Azzouzi, M., Maury, R.C., Charrière, A.,
 495 Taki, Z., Benammi, M., Michard, A., Hafid, M., Azzouzi, M. El, Maury, R.C., Charrière, A., Taki,
 496 Z., Benammi, M., Michard, A., 2008. The Atlas System, in: Michard, A., Saddiqi, O., Chalouan,
 497 A., Lamotte, D. de F. (Eds.), Continental Evolution: The Geology of Morocco. Lecture Notes in
 498 Earth Sciences 116. Springer, Berlin, Heidelberg, pp. 133 – 202. doi:10.1007/978-3-540-77076-
 499 3_4

500 Galdeano, A., Moreau, M.G., Pozzi, J.P., Berthou, P.Y., Malod, J.A., 1989. New paleomagnetic results
 501 from Cretaceous sediments near Lisboa (Portugal) and implications for the rotation of Iberia.
 502 Earth Planet. Sci. Lett. 92, 95 – 106. doi:10.1016/0012-821X(89)90024-1

503 García-Lasanta, C., Oliva-Urcia, B., Román-Berdiel, T., Casas, A.M., Hirt, A.M., 2014. Understanding
 504 the Mesozoic kinematic evolution in the Cameros basin (Iberian Range, NE Spain) from magnetic
 505 subfabrics and mesostructures. J. Struct. Geol. 66, 84 – 101. doi:10.1016/j.jsg.2014.05.013

506 García-Lasanta, C., Román-Berdiel, T., Oliva-Urcia, B., Casas, A.M., Gil-Peña, I., Speranza, F.,
 507 Mochales, T., 2015. Tethyan versus Iberian extension during the Cretaceous period in the eastern
 508 Iberian Peninsula: insights from magnetic fabrics. J. Geol. Soc. London. 2015 – 068.
 509 doi:10.1144/jgs2015-068

510 Gibbons, W., Moreno, T. (Eds.), 2002. The Geology of Spain. Geological Society of London.

511 Gil-Imaz, A., Pocoví-Juan, A., 1994. La esquistosidad alpina del extremo NW de la Cadena Ibérica
 512 Oriental (Sierra del Moncayo): Distribución, génesis y significado tectónico. Rev. Soc. Geol.
 513 España 7.

514 Golberg, J.M., Guiraud, M., Maluski, H., Séguret, M., 1988. Caractères pétrologiques et âge du
 515 métamorphisme en contexte distensif du bassin sur décrochement de Soria (Crétacé inférieur,

516 Nord Espagne). Comptes rendus l' Académie des Sci. Série 2 307, 521 – 527.

517 Gomez, F., Beauchamp, W., Barazangi, M., 2000. Role of the Atlas Mountains (northwest Africa)
 518 within the African-Eurasian plate-boundary zone. *Geology* 28, 775. doi:10.1130/0091-
 519 7613(2000)28<775:ROTAMN>2.0.CO;2

520 Gomez, M., Verges, J., Riaza, C., 2002. Inversion tectonics of the northern margin of the Basque
 521 Cantabrian Basin. *Bull. la Soc. Geol. Fr.* 173, 449 – 459. doi:10.2113/173.5.449

522 Gual-Pérez, J., Gil-Imáz, A., Simón-Gómez, J.L., 2012. Kinematic characterization of cleavage in
 523 Permo-Triassic red beds of the Espadán Range (Castellón , NE Spain). *Geogaceta* 51, 75 – 78.

524 Guitiérrez-Elorza, M., Pedraza-Gilsanz, J., 1974. Existencia de pizarrosidad alpina en la cordillera
 525 ibérica. *Boletín Geológico y Min.* 85, 269 – 270.

526 Hailwood, E. a., Mitchell, J.G., 1971. Palaeomagnetic and Radiometric Dating Results from Jurassic
 527 Intrusions in South Morocco. *Geophys. J. Int.* 24, 351 – 364. doi:10.1111/j.1365-
 528 246X.1971.tb02183.x

529 Henry, B., Rouvier, H., Le Goff, M., 2004. Using syntectonic remagnetizations for fold geometry and
 530 vertical axis rotation: the example of the Cévennes border (France). *Geophys. J. Int.* 157, 1061 –
 531 1070. doi:10.1111/j.1365-246X.2004.02277.x

532 Hirt, A.M., Lowrie, W., Pfiffner, O.A., 1986. A paleomagnetic study of tectonically deformed red beds
 533 of the Lower Glarus Nappe Complex, eastern Switzerland. *Tectonics* 5, 723 – 731.
 534 doi:10.1029/TC005i005p00723

535 Izquierdo-Llavall, E., Aldega, L., Cantarelli, V., Corrado, S., Gil-
 536 Peña, I., Invernizzi, C., Casas, A.M., 2013. On the origin of cleavage in the Central Pyrenees:
 537 Structural and paleo-thermal study. *Tectonophysics* 608, 303 – 318.
 doi:10.1016/j.tecto.2013.09.027

538 Jackson, M., Swanson-Hysell, N.L., 2012. Rock magnetism of remagnetized carbonate rocks: another
539 look. *Geol. Soc. London, Spec. Publ.* 371, 229 – 251. doi:10.1144/sp371.3

540 Juárez, M., Lowrie, W., Osete, M., Meléndez, G., 1998. Evidence of widespread Cretaceous
541 remagnetisation in the Iberian Range and its relation with the rotation of Iberia. *Earth Planet. Sci.*
542 *Lett.* 160, 729 – 743. doi:10.1016/S0012-821X(98)00124-1

543 Katz, B., Elmore, R.D., Cogoini, M., Engel, M.H., Ferry, S., 2000. Associations between burial
544 diagenesis of smectite, chemical remagnetization, and magnetite authigenesis in the Vocontian
545 trough, SE France. *J. Geophys. Res. Solid Earth* 105, 851 – 868. doi:10.1029/1999JB900309

546 Kirschvink, J.L., 1980. The least-squares line and plane and the analysis of paleomagnetic data.
547 *Geophys. Journal, R. Astron. Soc.* 62, 699 – 718. doi:10.1111/j.1365-246X.1980.tb02601.x

548 Kligfield, R., Lowrie, W., Hirt, A., Siddans, A.W.B., 1983. Effect of progressive deformation on
549 remanent magnetization of permian redbeds from the alpes maritimes (France). *Tectonophysics*
550 98, 59 – 85. doi:10.1016/0040-1951(83)90211-1

551 Laville, E., 1985. Evolution sédimentaire, tectonique et magmatique du bassin jurassique du Haut Atlas
552 (Maroc): modele en relais multiples de décrochements. Université de Montpellier.

553 Laville, E., Piqué, A., 1992. Jurassic penetrative deformation and Cenozoic uplift in the Central High
554 Atlas (Morocco): A tectonic model. structural and orogenic inversions. *Geol. Rundschau* 81,
555 157 – 170. doi:10.1007/BF01764546.

556 Laville, E., Zayane, R., Honnorez, J., Piqué, A., 1994. Le métamorphisme jurassique du Haut Atlas
557 central (Maroc) ; épisodes synschisteux et hydrothermaux. *Comptes rendus l' Académie des Sci.*
558 *Série 2. Sci. la terre des planètes* 318, 1349 – 1356.

559 Laville, E., Pique, A., Amrhar, M., Charroud, M., 2004. A restatement of the Mesozoic Atlasic Rifting
560 (Morocco). *J. African Earth Sci.* 38, 145 – 153. doi:10.1016/j.jafrearsci.2003.12.003

561 Liesa, C.L., Casas, A.M., Soria, A.R., Simón, J.L., Meléndez, A., 2004. Estructura extensional cretácica
562 e inversión terciaria en la región de Aliaga-Montalbán. *Geo-Guías* 1, 151 – 180.

563 Lüneburg, C.M., Lebit, H.D.W., 1998. The development of a single cleavage in an area of repeated
564 folding. *J. Struct. Geol.* 20, 1531 – 1548. doi:10.1016/S0191-8141(98)00039-X

565 Marshak, S., Mitra, G., 1988. *Basic methods of structural geology*. Prentice-Hall.

566 Mata, M.P., Casas, A.M., Canals, A., Gil, A., Pocovi, A., 2001. Thermal history during Mesozoic
567 extension and tertiary uplift in the Cameros basin, Northern Spain. *Basin Res.* 13, 91 – 111.
568 doi:10.1046/j.1365-2117.2001.00138.x

569 Mattauer, M., 1973. *Les Déformations des Matériaux de l'Ecorce Terrestre*. Hermann, Paris.

570 Mattauer, M., Tapponnier, P., Proust, F., 1977. Sur les mécanismes de formation des chaînes
571 intracontinentales. l'exemple des chaînes atlasiques du Maroc. *Bull. la Société géologique Fr.* 19,
572 321 – 326.

573 Michard, A., Ibouh, H., Charrière, A., 2011. Syncline-topped anticlinal ridges from the High Atlas: A
574 Moroccan conundrum, and inspiring structures from the Syrian Arc, Israel. *Terra Nov.* 23, 314 –
575 323. doi:10.1111/j.1365-3121.2011.01016.x

576 Mitra, G., Yonkee, W.A., 1985. Relationship of spaced cleavage to folds and thrusts in the Idaho-Utah-
577 Wyoming thrust belt. *J. Struct. Geol.* 7, 361 – 373. doi:10.1016/0191-8141(85)90041-0

578 Moreau, M.G., Ader, M., Enkin, R.J., 2005. The magnetization of clay-rich rocks in sedimentary basins:
579 low-temperature experimental formation of magnetic carriers in natural samples. *Earth Planet.*

580 Sci. Lett. 230, 193 – 210.

581 Moreau, M.G., Canerot, J., Malod, J.A., 1992. Paleomagnetic study of Mesozoic sediments from the
582 Iberian Chain (Spain); suggestions for Barremian remagnetization and implications for the
583 rotation of Iberia. Bull. la Soc. Geol. Fr. 163, 393 – 402.

584 Moussaid, B., Villalaín, J.J., Casas-Sainz, A., El Ouardi, H., Oliva-Urcia, B., Soto, R., Román-Berdiel,
585 T., Torres-López, S., 2015. Primary vs. secondary curved fold axes: Deciphering the origin of the
586 Aït Attab syncline (Moroccan High Atlas) using paleomagnetic data. J. Struct. Geol. 70, 65 – 77.
587 doi:10.1016/j.jsg.2014.11.004

588 Oliva-Urcia, B., Larrasoña, J.C., Pueyo, E.L., Gil, a., Mata, P., Parés, J.M., Schleicher, a. M., Pueyo,
589 O., 2009. Disentangling magnetic subfabrics and their link to deformation processes in cleaved
590 sedimentary rocks from the Internal Sierras (west central Pyrenees, Spain). J. Struct. Geol. 31,
591 163 – 176. doi:10.1016/j.jsg.2008.11.002

592 Oliva-Urcia, B., Pueyo, E.L., Larrasoña, J.C., 2008. Magnetic reorientation induced by pressure
593 solution: A potential mechanism for orogenic-scale remagnetizations, Earth and Planetary Science
594 Letters. doi:10.1016/j.epsl.2007.10.032

595 Oliva-Urcia, B., Román-Berdiel, T., Casas, A.M., Bógalo, M.F., Osácar, M.C., García-Lasanta, C.,
596 2013. Transition from extensional to compressional magnetic fabrics in the Cretaceous
597 Cabuérniga basin (North Spain). J. Struct. Geol. 46, 220 – 234. doi:10.1016/j.jsg.2012.09.001

598 Pevear, D.R., 1999. Illite and hydrocarbon exploration. Proc. Natl. Acad. Sci. U. S. A. 96, 3440 – 6.

599 Ramsay, J.G., Huber, M.I., 1987. Modern structural geology, Volume 2: Folds and Fractures. Academic
600 Press, London.

601 Saura, E., Verges, J., Martin-Martin, J.D., Messenger, G., Moragas, M., Razin, P., Grelaud, C.,

602 Joussiaume, R., Malaval, M., Homke, S., Hunt, D.W., 2014. Syn- to post-rift diapirism and
 603 minibasins of the Central High Atlas (Morocco): the changing face of a mountain belt. *J. Geol.*
 604 *Soc. London.* 171, 97 – 105. doi:10.1144/jgs2013-079

605 Schaer, J.J., Persoz, F., 1976. Aspects structuraux et pétrographiques du Haut Atlas calcaire de Midehr
 606 (Maroc). *Bull. La Soc. Geol. Fr.* 7, 1239 – 1250.

607 Schaer, J.P., 1987. Evolution and structure of the High Atlas of Morocco, in: Schaer, J.P., Rodgers, J.
 608 (Eds.), *The Anatomy of Mountain Ranges*. Princeton University Press, pp. 107 – 128.

609 Séguret, M., 1972. Etude tectonique des nappes et series decollées de la partie centrale du versant sud
 610 des Pyrénées. Caractère sédymентаire, rôle de la compression et de la gravité. Université des
 611 Sciences et Techniques du Languedoc (Montpellier II).

612 Shipunov, S. V, 1997. Synfolding magnetization: detection, testing and geological applications.
 613 *Geophys. J. Int.* 130, 405 – 410.

614 Soto, R., Villalain, J.J., Casas-Sainz, A.M., 2008. Remagnetizations as a tool to analyze the tectonic
 615 history of inverted sedimentary basins: A case study from the Basque-Cantabrian basin (north
 616 Spain). *Tectonics* 27, TC1017. doi:10.1029/2007TC002208 Soto, R., Casas-Sainz, A.M., Villalain,
 617 J.J., 2011. Widespread Cretaceous inversion event in northern Spain: evidence from subsurface
 618 and palaeomagnetic data. *J. Geol. Soc. London.* 168, 899 – 912. doi:10.1144/0016-76492010-072

619 Teixell, A., Arbolea, M.-L., Julivert, M., Charroud, M., 2003. Tectonic shortening and topography in
 620 the central High Atlas (Morocco). *Tectonics* 22, n/a – n/a. doi:10.1029/2002TC001460

621 Torres-Lopez, S., Villalain, J.J., Casas, A.M., EL Ouardi, H., Moussaid, B., Ruiz-Martinez, V.C., 2014.
 622 Widespread Cretaceous secondary magnetization in the High Atlas (Morocco). A common origin
 623 for the Cretaceous remagnetizations in the western Tethys? *J. Geol. Soc. London.* 171, 673 – 687.

doi:10.1144/jgs2013-107

Torres-López, S., Casas, A.M., Villalaín, J.J., El Ouardi, H., Moussaid, B., 2016. Pre-Cenomanian vs. Cenozoic folding in the High Atlas revealed by palaeomagnetic data. *Terra Nov.* 28, 110 – 119. doi:10.1111/ter.12197

Torsvik, T.H., Van der Voo, R., Preeden, U., Niocaill, C. Mac, Steinberger, B., Doubrovine, P. V., van Hinsbergen, D.J.J., Domeier, M., Gaina, C., Tohver, E., Meert, J.G., McCausland, P.J. a, Cocks, L.R.M., 2012. Phanerozoic polar wander, palaeogeography and dynamics. *Earth-Science Rev.* 114, 325 – 368. doi:10.1016/j.earscirev.2012.06.002

Van Der Voo, R., Torsvik, T.H., 2012. The history of remagnetization of sedimentary rocks: deceptions, developments and discoveries. *Geol. Soc. London, Spec. Publ.* 23 – 53. doi:10.1144/SP371.2

Villalaín, J., Fernández-González, G., Casas, A., Gil-Imaz, A., 2003. Evidence of a Cretaceous remagnetization in the Cameros Basin (North Spain): implications for basin geometry. *Tectonophysics* 337, 101 – 117. doi:10.1016/j.tecto.2003.08.024

Villalaín, J.J., Casas-Sainz, A.M., Soto, R., 2015. Reconstruction of inverted sedimentary basins from syn-tectonic remagnetizations. A methodological proposal. *Geol. Soc. London, Spec. Publ.* 425. doi:10.1144/SP425.10

Waldhör, M., Appel, E., 2006. Intersections of remanence small circles: New tools to improve data processing and interpretation in palaeomagnetism. *Geophys. J. Int.* 166, 33 – 45. doi:10.1111/j.1365-246X.2006.02898.x

Williams, P.F., 1985. Multiply deformed terrains—problems of correlation. *J. Struct. Geol.* 7, 269 – 280. doi:10.1016/0191-8141(85)90035-5

Winklhofer, M., Fabian, K., Heider, F., 1997. Magnetic blocking temperatures of magnetite calculated

with a three-dimensional micromagnetic model. *J. Geophys. Res.* 102, 22695 – 22709.
doi:10.1029/97JB01730

Figure captions

Fig. 1. Schematic map showing the western Tethys domain and the Mesozoic intracratonic basins in which remagnetizations have been observed: Basque-Cantabrian basin (Soto et al., 2008), Cameros (Villalaín et al., 2003), Aragonese Branch (Juárez et al., 1998), Maestrazgo (Moreau et al., 1992), Lusitanian basin (Galdeano et al., 1989), Middle Atlas (Calvín et al., in review), Central High Atlas (Torres-López et al., 2014; Moussaid et al., 2015).

Fig. 2. Geologic map of the study area showing the paleomagnetic sites used in this work (see also supplementary data).

Fig. 3. Photographs showing representative structures in the study area (see text for explanation).

Fig. 4. Photographs showing the geometry of cleavage at the outcrop scale and its relationship with bedding (see text for details).

Fig. 5. Thin-sections photographs showing the morphology of cleavage at the microscale. Solid (black or white) line shows the general attitude of the cleavage and dashed line corresponds with the

bedding. Arrows are in relation with the text explanations

Fig. 6. Lower hemisphere, equal-area stereoplots showing structural data. a) Poles from bedding and paleo-bedding (black circles and red diamonds, respectively) and cylindrical best fit for each dataset (cylindrical best fit for paleo-bedding was calculated only with the 24 data whose paleo-dip was at least the 70% of the total dip). b) poles of foliation and mean foliation plane (solid plane), mean vector (and associated $\alpha 95$) and cylindrical best fit. Note that cylindrical best fit are similar between both bedding datasets but not for foliation.

Fig. 7. Orthogonal plot of NRM thermal demagnetization of representative samples in geographic coordinates of a) red beds and b) limestones. Solid black symbols are projected onto the horizontal plane (N towards the left and W towards the down) and open symbols onto the vertical E-W plane). Purple dashed line show the remagnetization component. Normalized NRM intensity is shown.

Fig. 8. Equal-area projection (lower hemisphere) of paleomagnetic directions (with $\alpha 95$) in a) GEO and b) TILT coordinates (before and after bedding correction respectively). c) contours of equal value of the parameter A/N (Waldh r and Appel, 2006) calculated for these data (Table 1). d) Optimal paleomagnetic direction and its corresponding small circles.

Fig. 9. Present-day and restored cross-section of the a) Timarirhine and b) Tissila areas. Arrows indicate the paleomagnetic inclination in each site before and after the correction at the Albian-

Cenomanian paleomagnetic direction. See location of the cross-sections in Fig. 2.

Fig. 10. Key outcrops showing post-remagnetization folds with axial-plane cleavage (a,b) and plane-view sketch of a pre-remagnetization fold and post-folding cleavage (c).

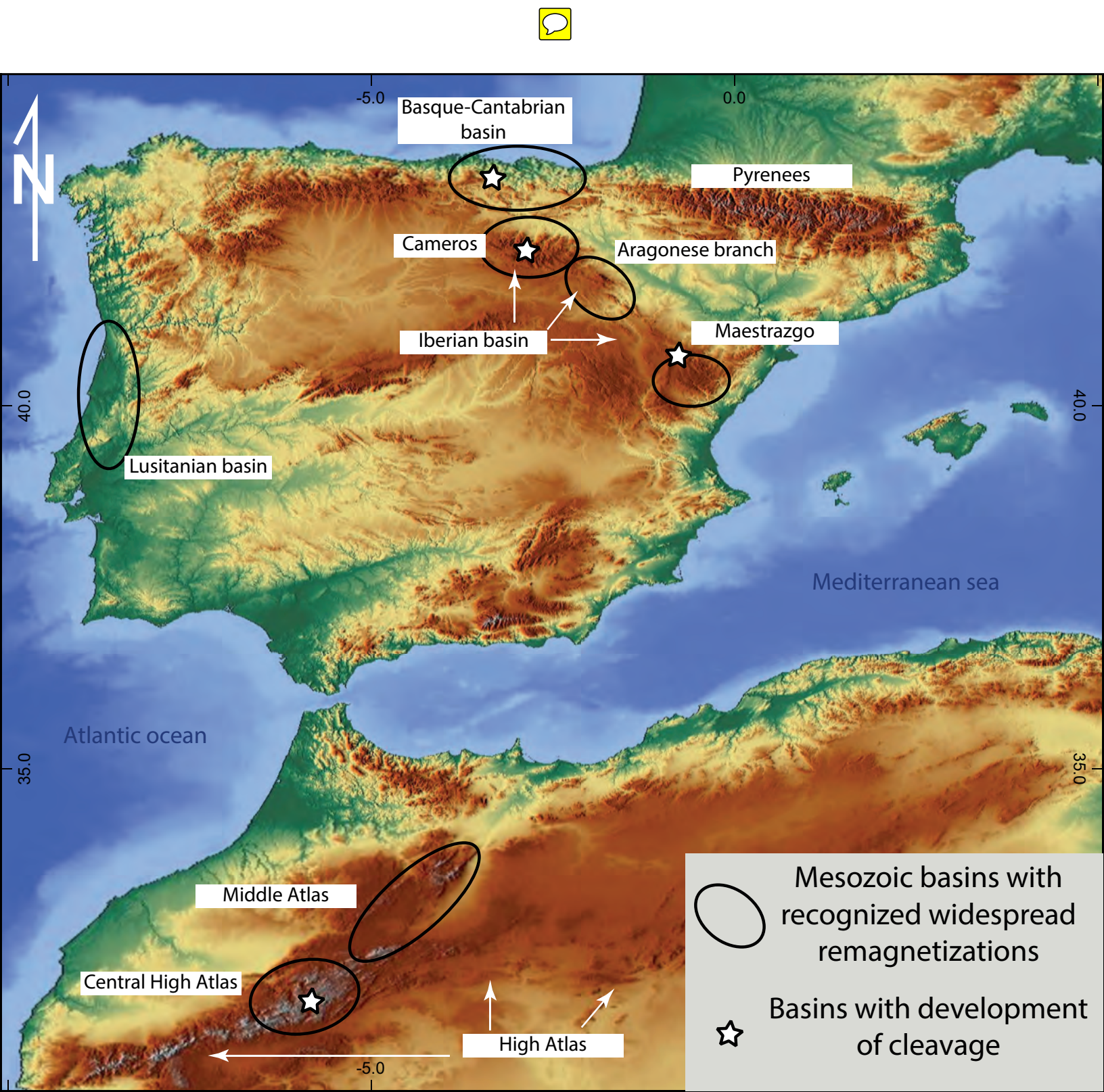
Fig. 11. Schematic geological map of the Outerbat sector showing relationships between different structures: bedding, cleavage, folds and dikes. a) Present day attitude; note that dikes cut across bedding and that bedding-cleavage relationship vary along the structure. b) Map with paleo-bedding. c) Lower hemisphere, equal-area stereoplots showing structural data (S1: cleavage, So: bedding, paleo-So: paleo-bedding) and cylindrical best fit of each data-set. d) Paleomagnetic direction (Geo, Tilt and BFD) and associated small-circle for each site.

Fig. 12. General, idealized cross section of the studied area projecting foliation data onto the plane of the section.

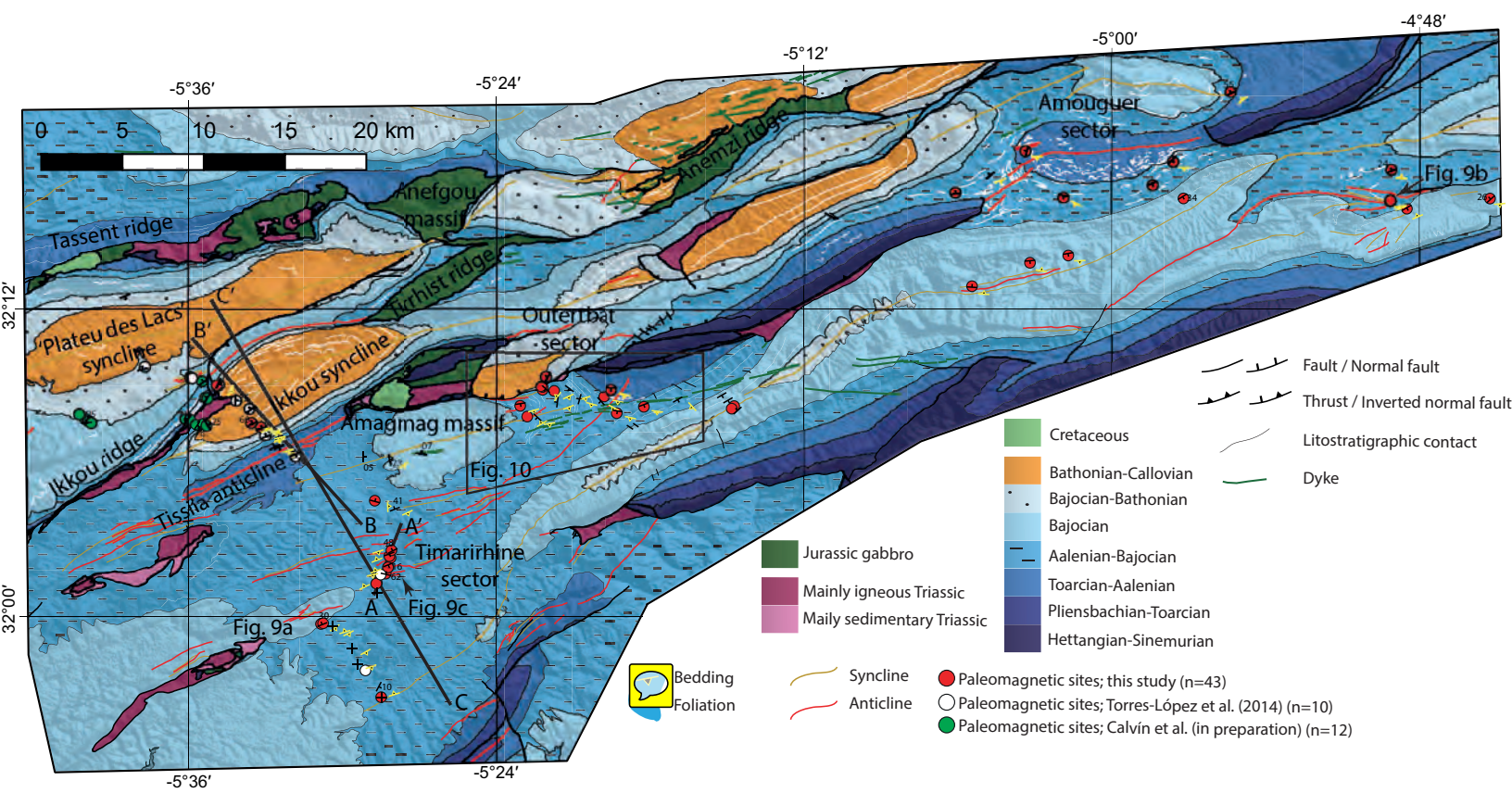
Tables

Table 1. n/N: number of samples used to calculate the paleomagnetic direction / number of measured samples. Lit: sample lithology (Car: carbonate rocks -limestones and marls-, Rb: red beds -sandstones and shales-). α_{95} and κ , Fisher statistical parameters (Fisher, 1953). BFD-expec dir angle: angle between the calculated best fit direction in each site and the calculated reference paleomagnetic direction for the area. Ref: literature reference of the data (A, this work; B, Torres-López et al. 2014; C, Calvín et al. (in preparation). For coordinates of each site, see supplementary material.

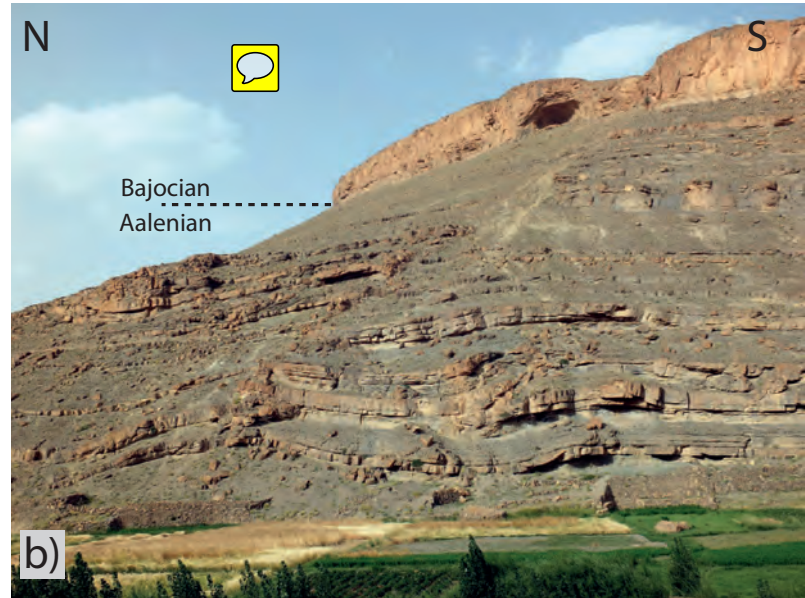
Figure



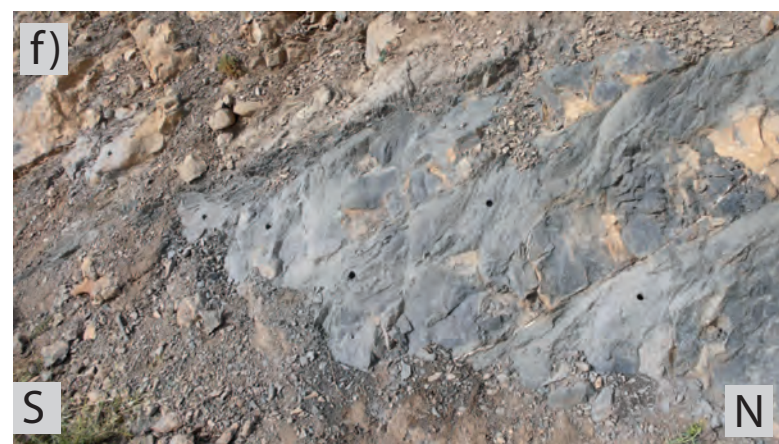
Figure



Figure

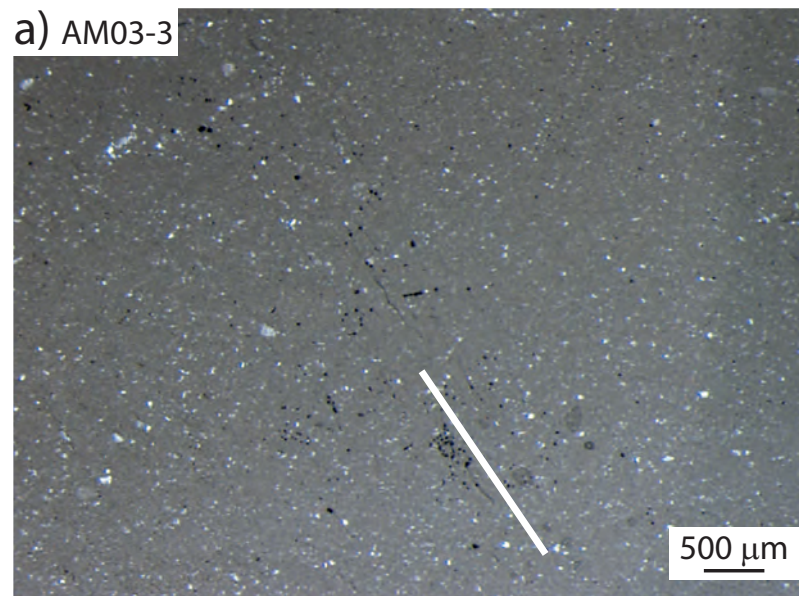


Figure

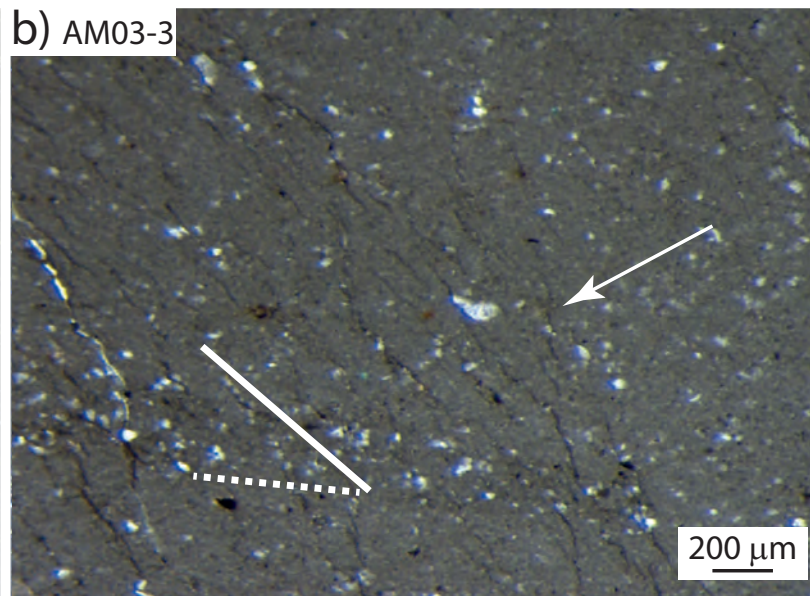


Figure

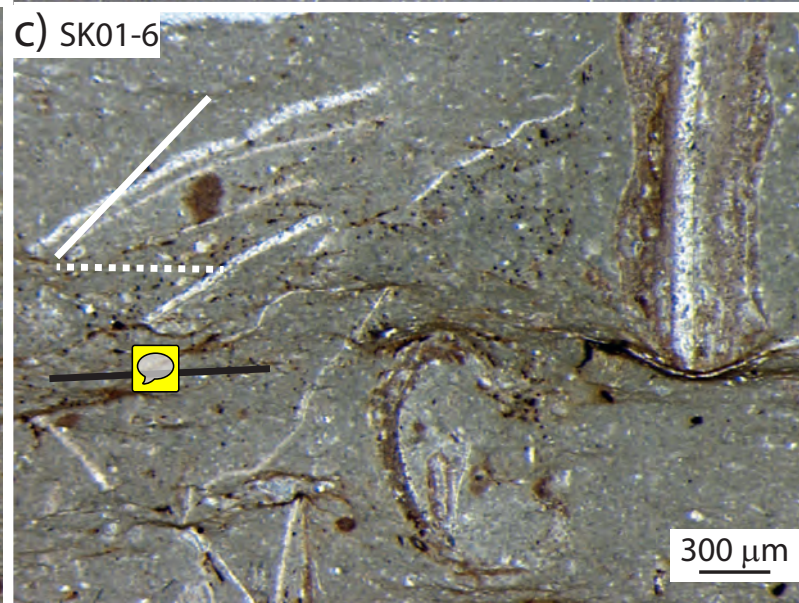
a) AM03-3



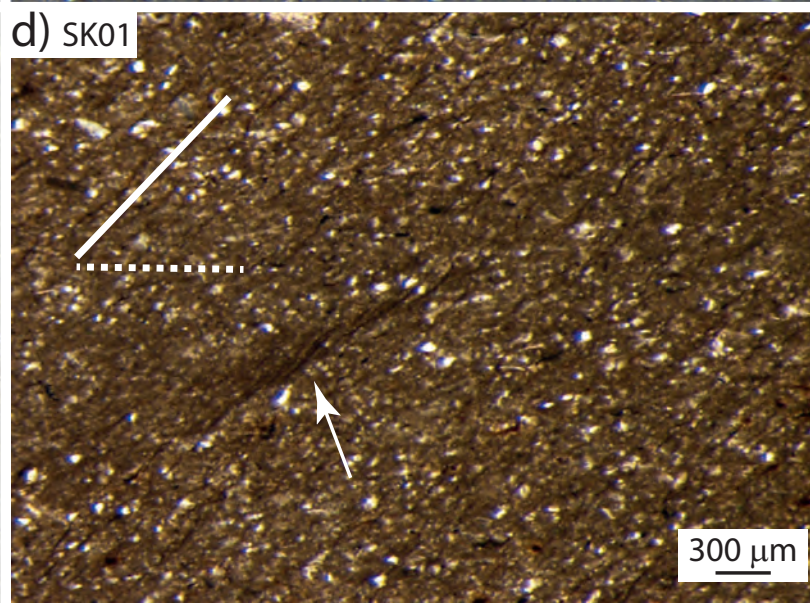
b) AM03-3



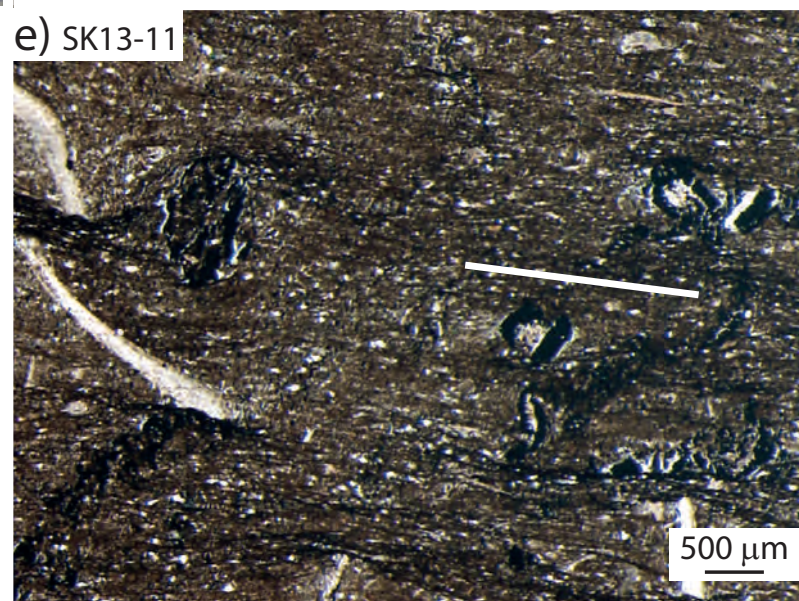
c) SK01-6



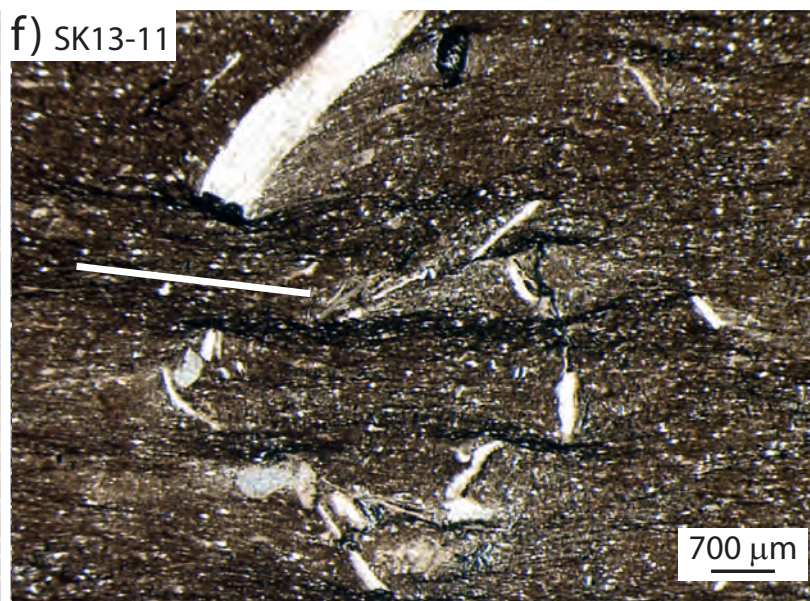
d) SK01



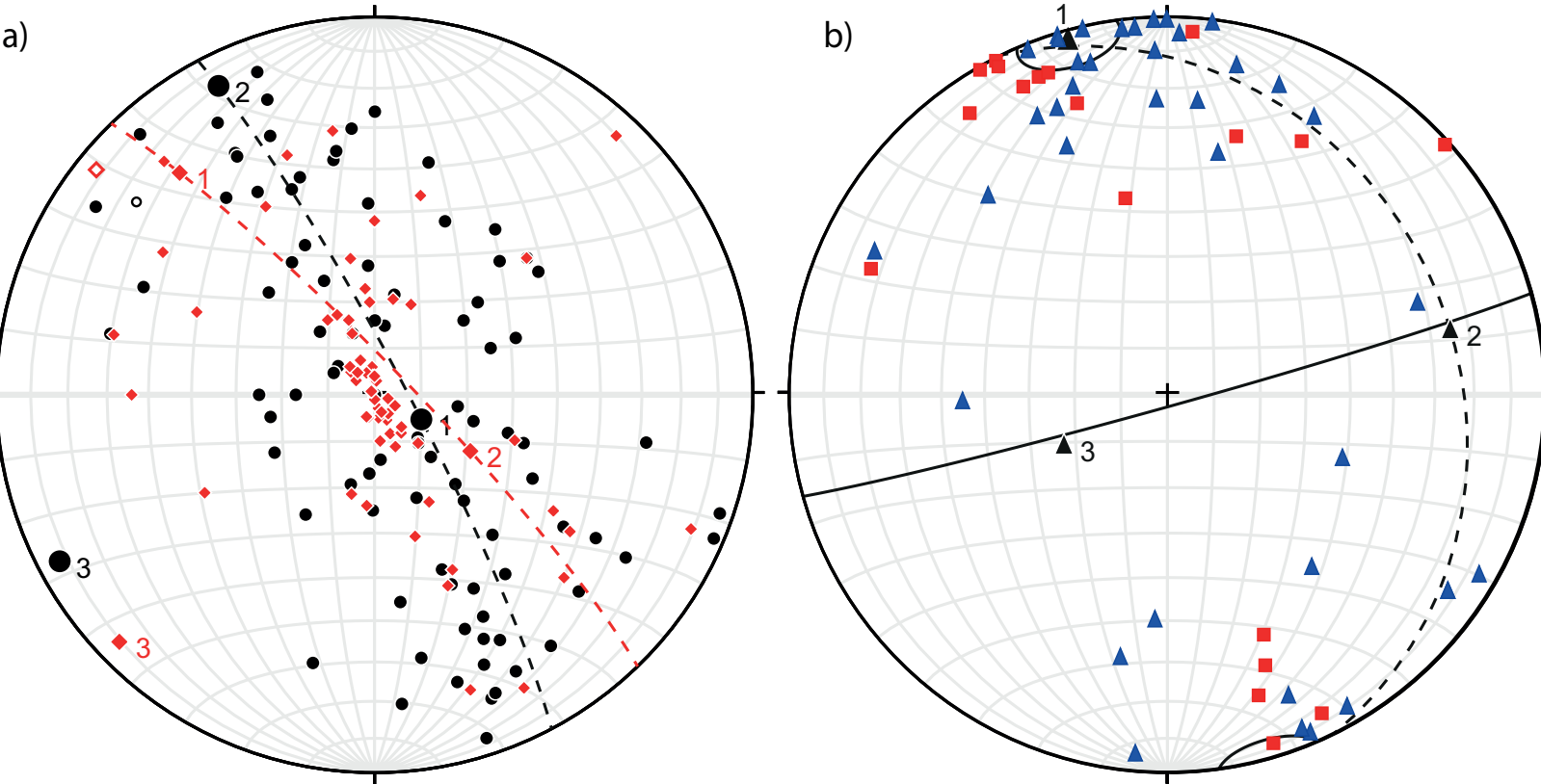
e) SK13-11



f) SK13-11



Figure

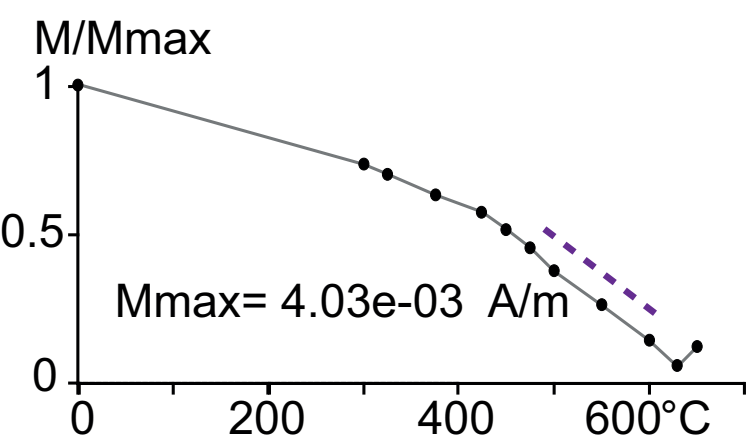
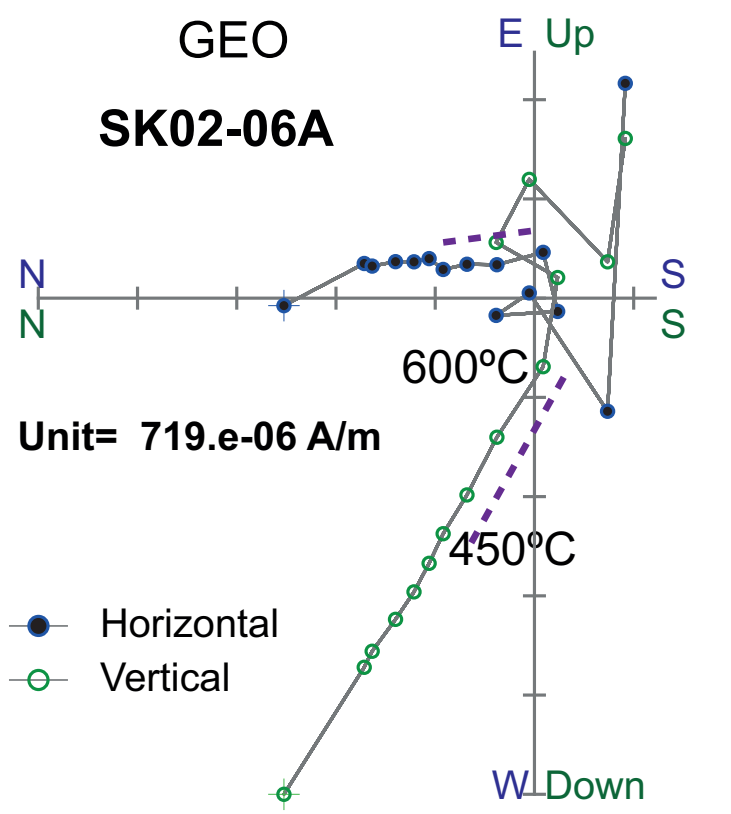


Bedding (black circles, n=95)
Paleo-bedding (red diamonds, n=65)

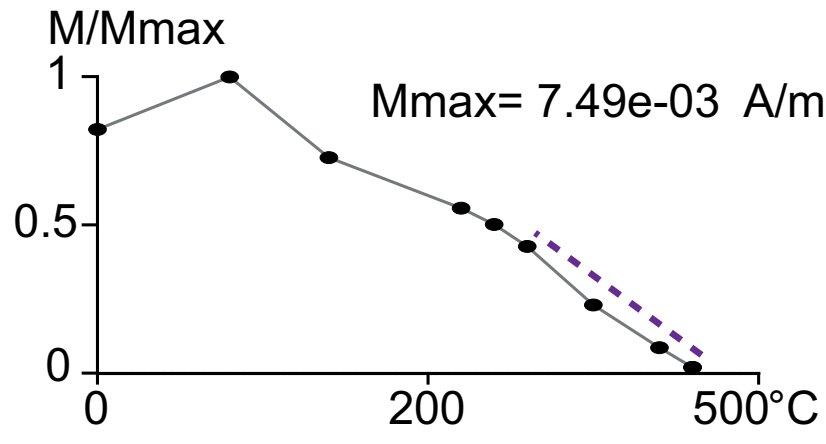
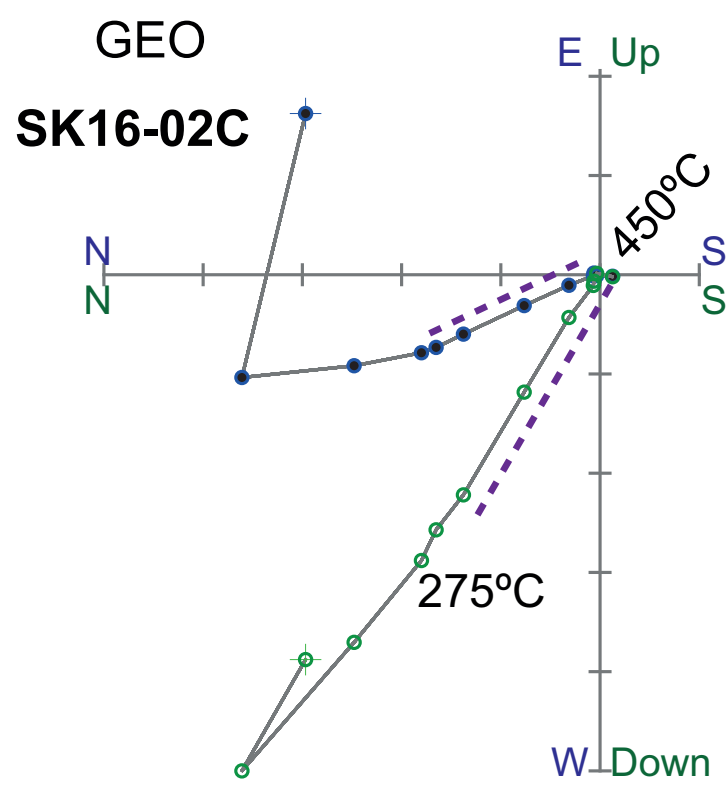
Cleavage Tissila-Amouguer sector (triangles, n=40)
Cleavage Timarirhine sector (cubes, n=19)

Figure

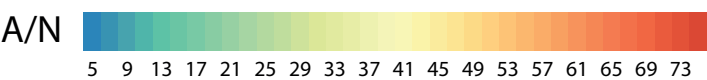
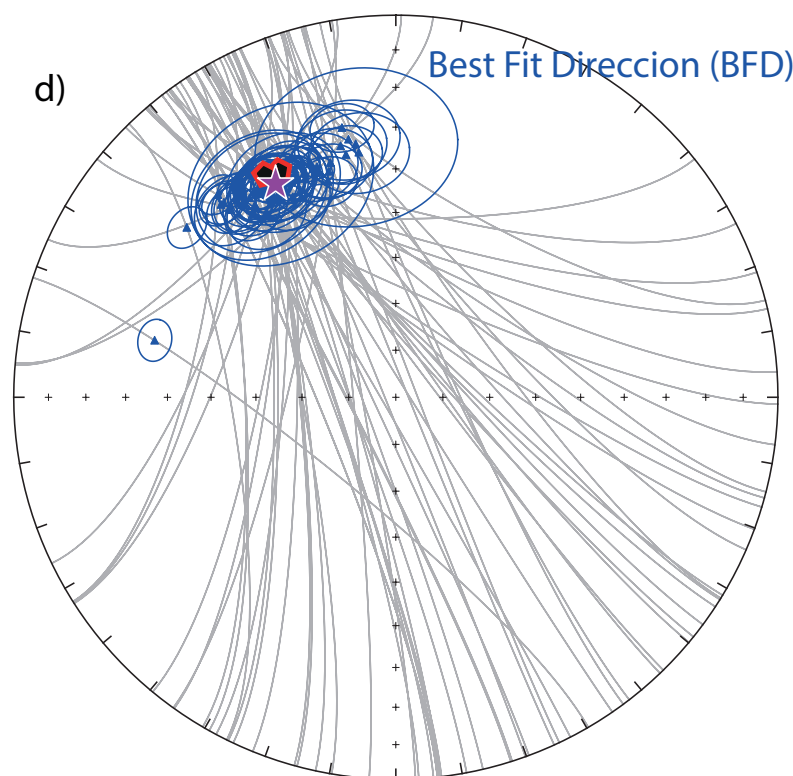
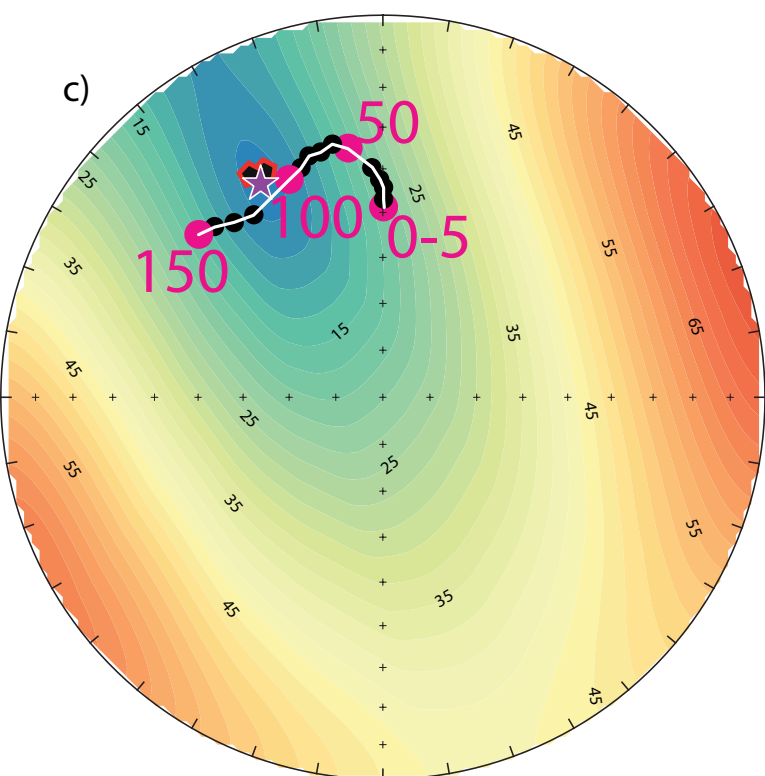
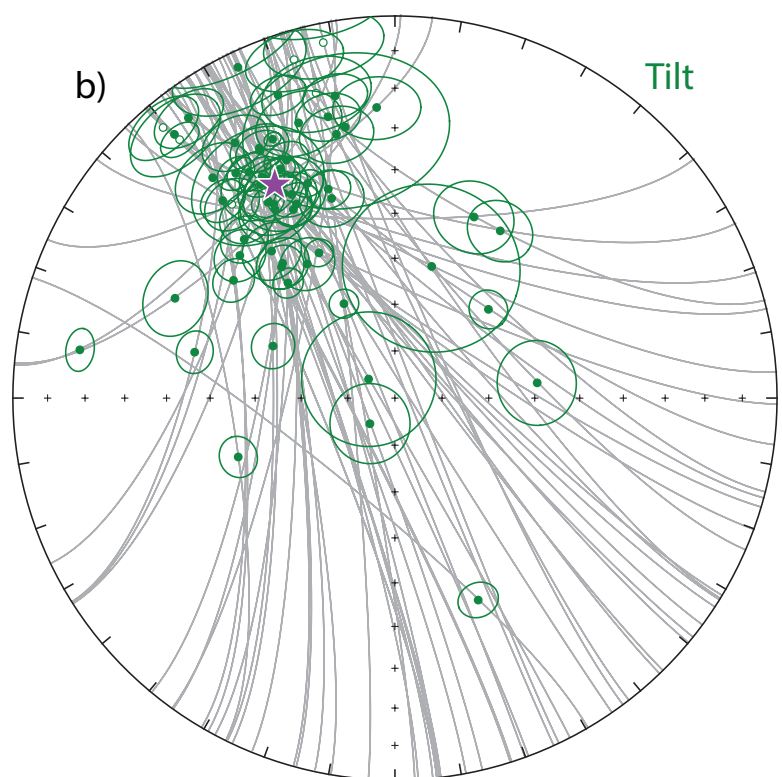
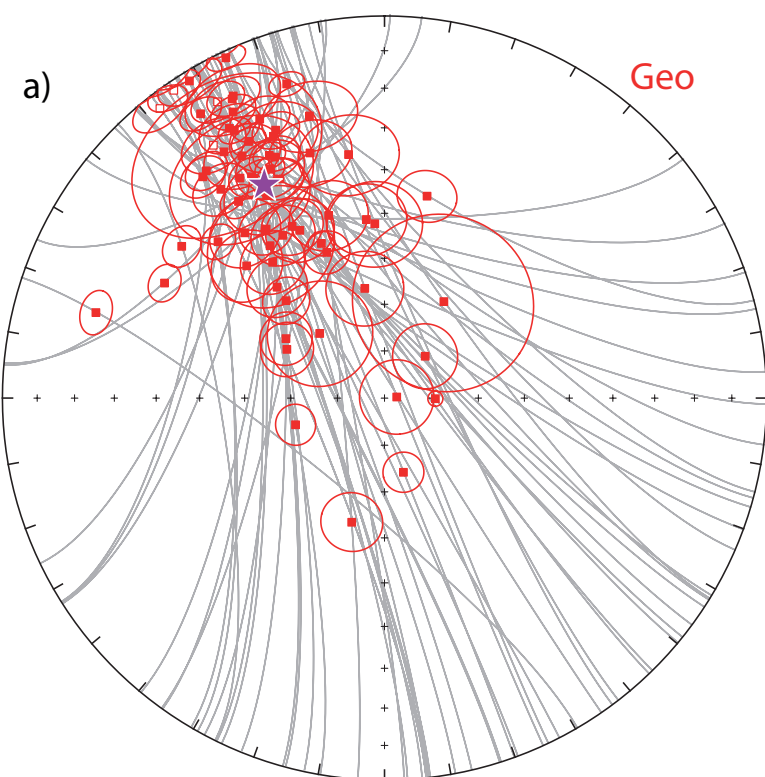
a) Red bed



b) Limestone



Figure

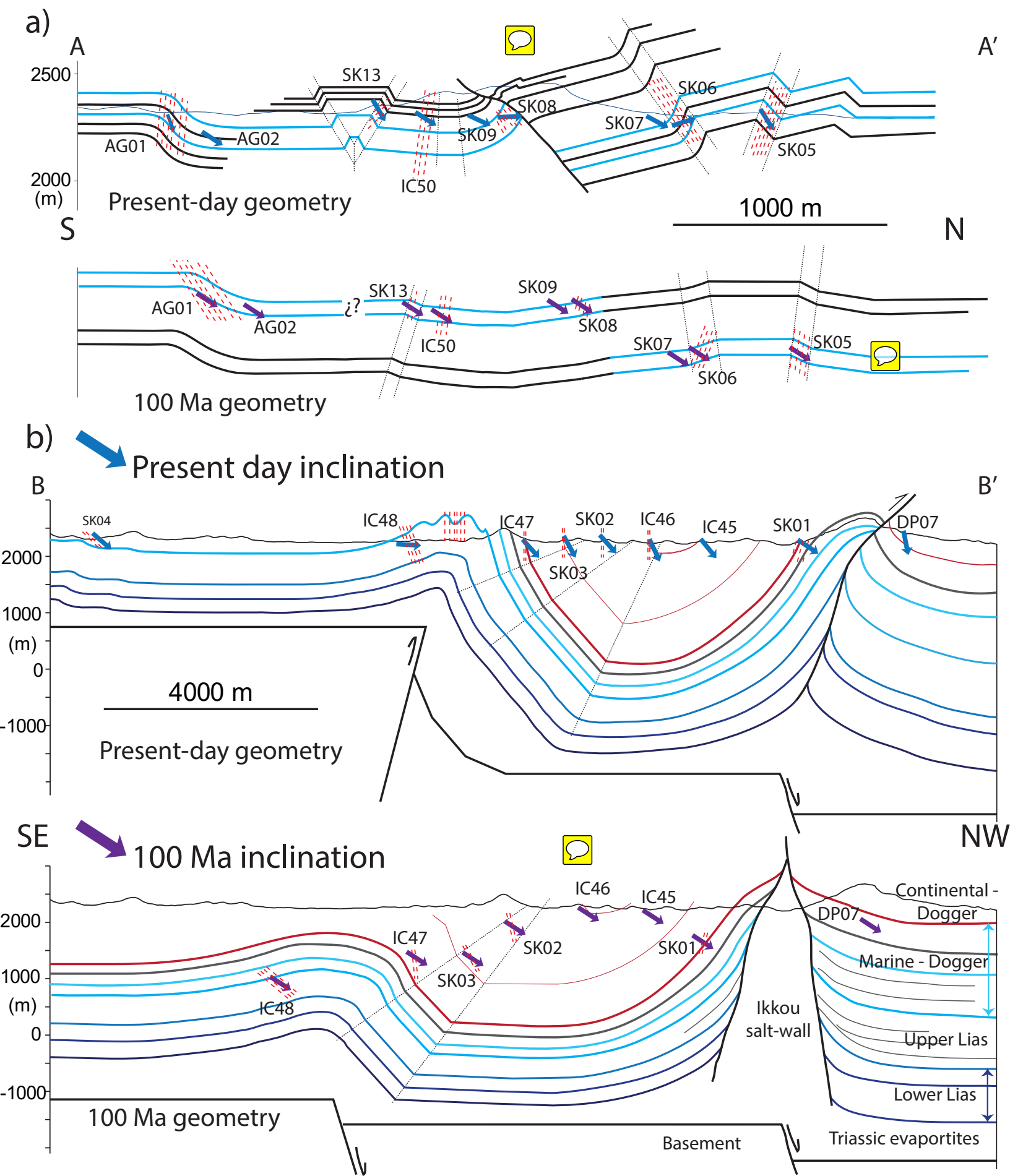


★ Direction of the remagnetization (D: 330.6, I: 36.1)

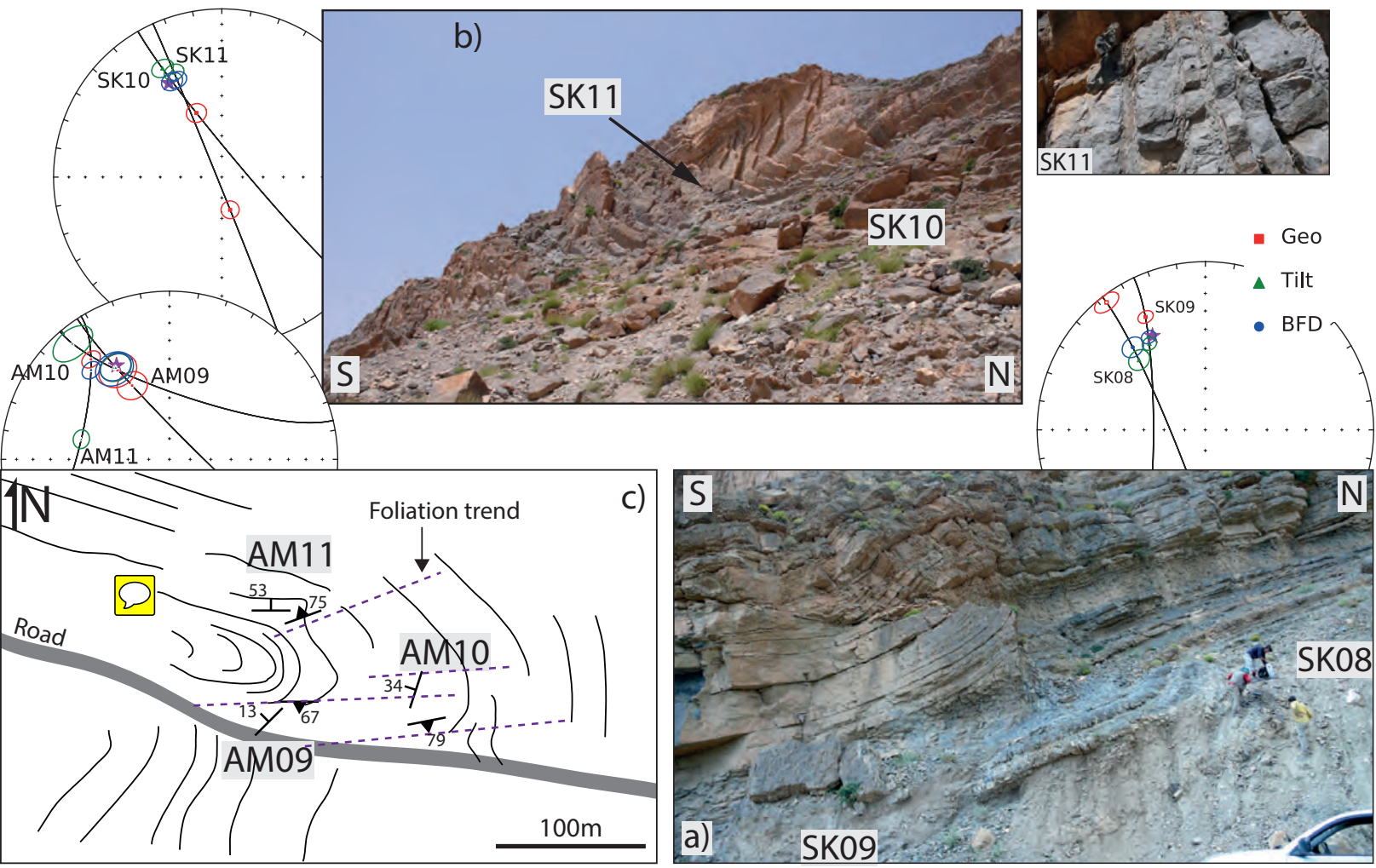
◆ Horizontal-Bedding sites

● Expected direction from Torsvik 2012 (Ma)

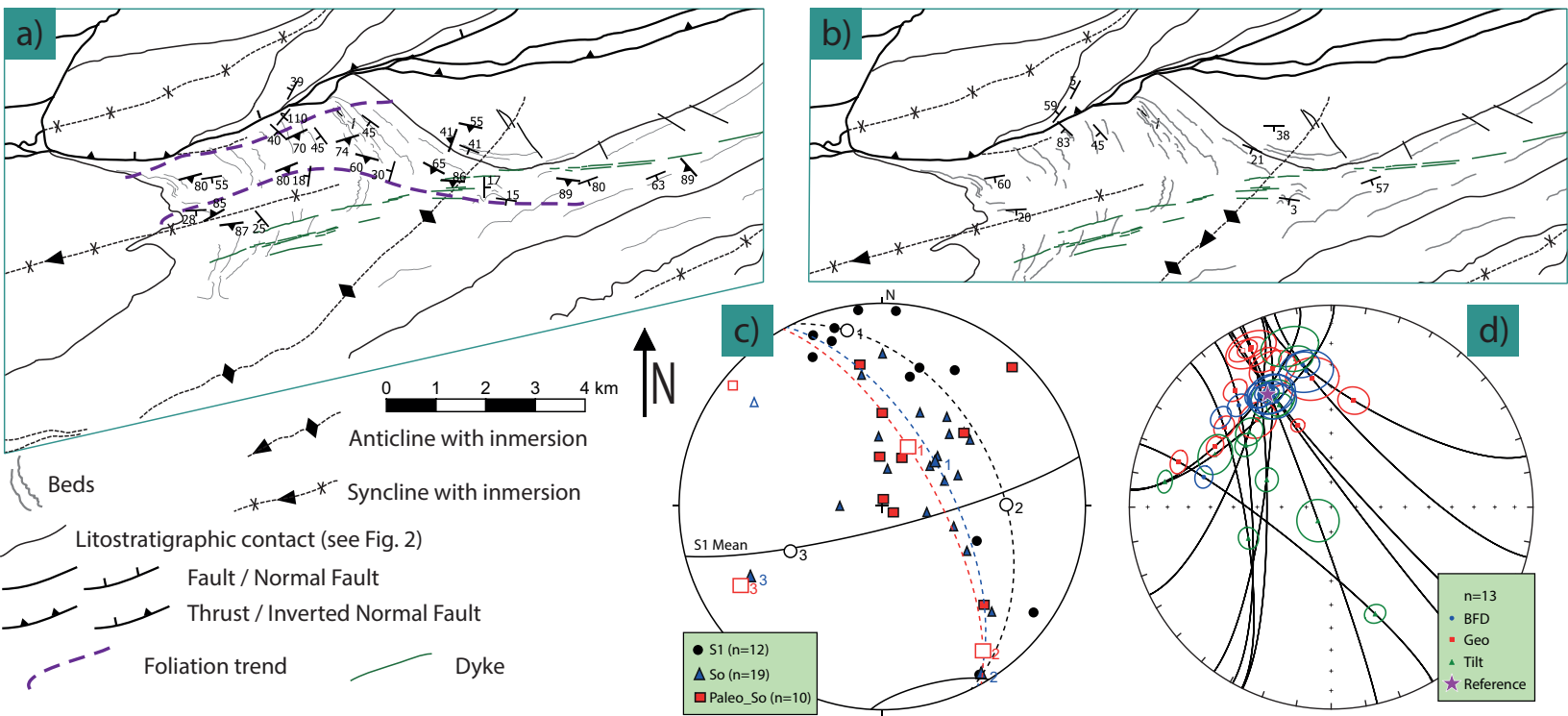
Figure



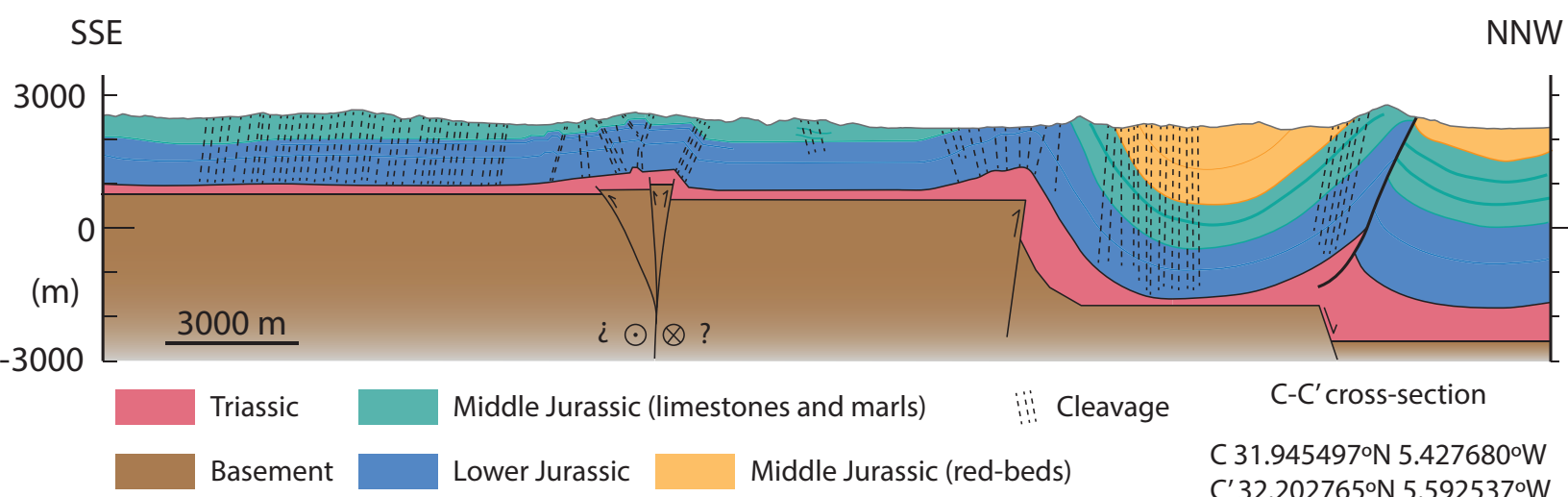
Figure



Figure



Figure



Table

Site	n/N	Lit	In situ (GEO)		alfa_95	k	100 % corrected (TILT)		Best Fir Direction		BFD-expec.dir	Bedding	Paleo-bedding	Ref
			DEC	INC			DEC	INC	DEC	INC		DipDir/Dip	DipDir/Dip	
AG01	6/6	Car	314.9	70.5	11.2	36.7	334.6	4.7	332.4	36.4	1.4	344/68	344/32	A
AG02	6/6	Car	329	32.9	4.5	219.4	329	32.9	328.4	35.9	1.8	344/00	344/03	A
AM01	8/8	Car	335.5	31.3	4.9	130.1	338.9	16.1	333.3	37	2.3	004/17	004/24	A
AM02	8/8	Car	335	2	3.2	293.6	317.1	56.2	330	36.1	0.5	175/60	175/23	A
AM03	8/8	Car	342.7	15	3.1	316.6	331.6	67.1	341.1	37.5	8.5	170/53	170/30	A
AM04	8/8	Car	334.5	36.6	4.7	138.6	319.1	52.6	334	37.5	3	191/22	191/21	A
AM05	8/8	Car	44.2	77.6	6.9	64.7	347.5	30	348.3	35.4	14.4	334/55	334/06	A
AM06	8/8	Car	327.1	12.4	3.8	185.9	331.7	43.3	329.9	36.3	0.6	134/32	134/07	A
AM07	6/8	Car	331.7	47.7	6.3	114	327.9	22.2	329.4	36.3	1	318/26	318/14	A
AM08	7/8	Car	326.7	31.7	14.3	18.8	305.8	83.1	326.5	36.2	3.3	150/52	150/48	A
AM09	5/6	Car	333.2	49.3	7	120.3	329.7	36.8	329.6	36.3	0.8	315/13	135/01	A
AM10	4/4	Car	329.8	38.6	8.6	114.2	320.1	11	328.7	37	1.8	288/34	288/32	A
AM11	5/5	Car	321.9	25.4	4.2	327.7	282.9	45.3	318.7	30	11.7	193/53	193/45	A
AM12	8/8	Car	313.8	48.6	7.6	54.1	320.4	26.1	318.7	34.9	9.8	338/24	338/09	A
AM13	8/8	Car	330.7	20.8	3	350.9	332.4	54.7	331.1	36.2	0.4	148/34	148/19	A
AM14	8/8	Car	301.1	65.4	5.6	97.5	331.5	26.5	329.1	35.9	1.2	353/46	353/10	A
AM15	8/8	Car	343	48.6	7.9	50.4	327.8	34.3	329.4	36.8	1.2	285/22	285/03	A
AM16	6/8	Car	330.1	19.7	5.7	139.9	326.8	55.5	329.3	36.1	1.1	155/36	155/19	A
DP01	8/8	Car	194.8	62.5	6.4	75.5	342.4	44.4	343.5	38.2	10.5	355/71	175/06	B
DP02	8/8	Car	253.3	70.2	4.3	166.7	327.1	30.3	325.7	35.3	4.1	350/60	350/05	B
DP03	7/8	Car	314.7	60.3	5	144.4	333.1	40	334.3	37.2	3.1	001/25	181/03	B
DP04	8/8	Car	320.5	52	6.8	68.1	328	39.9	329.5	36	0.9	355/14	175/04	B
DP05	8/8	Car	325	45.1	5.6	99.2	319.9	-34.1	321.8	39	7.6	293/87	293/80	B
DP06	8/8	Car	328	48.4	6.6	70.4	319.4	-7.5	323.8	37.7	5.7	303/59	303/47	B
DP07	8/8	Car	90.7	79.2	1.6	1178.8	334.7	26	335.8	35.8	4.2	325/70	325/10	B
DP08	7/8	Car	345.1	24.6	8.7	48.8	83.9	59.3	347.6	33.1	14.3	138/82	138/72	B
DP09	8/8	Car	332.1	16.4	4.1	185.7	46.5	62.4	337.2	34.4	5.6	124/78	124/57	B
DP10	7/8	Car	321.9	31.2	5.7	115.1	320.8	-38.7	321.3	35.7	7.6	333/71	333/76	B
DP11	8/8	Car	323.4	36.1	3.7	219.5	320.2	-13	323.8	37.6	5.7	305/51	305/53	B
DP12	5/8	Rb	343.1	33.4	7.9	94.1	356.4	24.8	330.6	35.6	0.5	060/25	060/43	B
IC02	7/8	Car	325.6	-2.7	4.6	170.4	318.9	32	318.6	32.5	10.6	178/42	358/01	C
IC03	7/8	Car	85	87.4	7.9	59	340.7	24.7	341.1	36.4	8.4	338/66	338/12	C
IC44	7/8	Car	326.9	24.1	18.4	11.7	15.6	60.7	331.5	35.9	0.8	115/57	115/43	C
IC45	7/8	Rb	354.2	51.2	8.1	56.1	23.6	47.1	325.1	40.5	6.2	090/25	090/54	C
IC46	7/8	Rb	31.6	65.8	19.1	10.9	349.6	28.7	351	33.3	16.9	324/49	324/05	C
IC47	8/8	Car	323.1	48.7	13.2	18.6	327.1	-33.8	326.7	35.8	3.2	342/85	342/71	C
IC48	7/8	Car	328.4	2.9	5.5	119.9	320.2	52.1	325.5	35.6	4.2	161/51	161/17	C

IC50	9/10	Car	334.6	30.4	3.1	273.1	337.9	39.2	336.1	35	4.6	128/10	128/05	C
IC51	9/10	Car	337.9	25.3	4.4	136.6	342.3	42.1	339.9	34.9	7.7	139/18	139/08	C
OU01	8/8	Car	319.8	42.8	7.4	57.5	294.4	36.9	332.9	40.6	4.9	228/30	228/45	A
OU02	6/8	Car	11.9	45.1	5.9	131.7	346.6	25.3	348.7	28.8	16.9	298/39	298/05	A
OU03	6/8	Car	351.6	35.8	9.6	50.1	345.5	-18.7	349.6	31.8	16.3	314/64	314/59	A
OU04	8/8	Car	286.5	22.3	4	190.1	157.6	42.3	283.3	35.4	38.1	129/110	129/96	A
OU05	8/8	Car	297.6	35.3	3.7	223.2	278.7	17.7	329.7	34.8	1.5	223/40	223/83	A
OU06	8/8	Car	337	26.5	8.3	45.2	331.6	39	332.8	37	1.9	188/15	188/03	A
OU07	5/8	Car	333	13.2	8.5	82.4	224.3	82.4	331.5	36.3	0.8	160/80	160/57	A
SK01	7/8	Car	333.4	33.4	6.7	82.8	32.2	47.1	334.1	34.3	3.4	103/61	103/60	A
SK02	6/8	Rb	356.8	52.3	9.6	49.6	348.6	-5.7	351.4	35.3	16.9	336/60	336/42	A
SK03	7/8	Rb	349.8	66.2	8.1	56.4	343.4	-8.4	344.4	36.4	11.1	339/75	339/45	A
SK04	8/8	Car	313.2	40	3.7	228.2	324.7	28.7	322.4	31.9	8.1	015/20	015/05	A
SK05	8/8	Car	315.9	56.8	6.4	76.7	323.6	9.8	321.6	35.7	7.3	333/48	333/26	A
SK06	7/7	Car	325.9	-21.2	6.2	94.8	320	48.4	323.8	35.5	5.6	160/72	160/14	A
SK07	8/8	Car	329.5	27.3	7.4	57.2	327.6	41	328.5	36	1.8	160/14	160/05	A
SK08	7/8	Car	322.2	-4.6	5	144.3	316.5	42.2	318.7	34.9	9.8	158/49	158/08	A
SK09	7/7	Car	332.1	25	3.3	335.8	327	38.8	328.5	35.6	1.8	180/16	180/04	A
SK10	8/8	Car	338.4	56.3	4.7	141.5	331.4	27.2	332.5	36	1.5	320/30	320/09	A
SK11	8/8	Car	165.7	73.7	4.3	167.7	335.5	32.1	335.3	36.4	3.8	338/74	338/04	A
SK12	8/8	Car	333.4	33.4	2.9	366.1	333.4	33.4	331.1	36.4	0.5	020/00	020/05	A
SK13	8/8	Car	296.5	66.7	5.7	96.2	348.8	20.5	342.6	40.5	10.4	013/62	013/22	A
SK14	8/8	Car	333.4	12.6	4.7	140	293.1	61.6	327.6	35.3	2.6	180/64	180/38	A
SK15	8/8	Car	335.9	21.1	5.5	102.7	312.6	44.1	327.5	34.3	3.1	202/41	202/21	A
SK16	8/8	Car	337.8	54	2.7	404.8	332.4	36.8	332.3	36	1.3	318/18	138/01	A
SK17	7/8	Car	330.6	-12	4.8	159	333.1	42.5	332.2	36.1	1.3	143/55	143/06	A
SK18	8/8	Car	306.8	34.1	4.2	174.3	249.4	53.9	309.1	30.2	18.9	171/55	171/60	A
SK19	8/8	Car	320.6	26	4.5	149.4	306.1	46.6	317.8	32.4	11.2	177/28	177/20	A

Interactive Map file (.kml or .kmz)

[Click here to download Interactive Map file \(.kml or .kmz\): Supplementary.kmz](#)